Proceedings of the Project Review, Geo-Mathematical Imaging Group (Purdue University, West Lafayette IN), Vol. 1 (2014) pp. 389-415.

D-BAR METHOD AND EXCEPTIONAL POINTS AT POSITIVE ENERGY: A COMPUTATIONAL STUDY

JANNE P. TAMMINEN*, MAARTEN V. DE HOOP†, MATTI LASSAS‡, AND SAMULI SILTANEN§

Abstract. A new computational method for reconstructing a potential at positive energy is developed. The method is based on the D-bar method which has no exceptional points if the potential is small enough compared to the energy. Numerical tests show exceptional points for perturbed, radial potentials. Reconstructions for radial and non-radial potentials are computed using simulated Dirichlet-to-Neumann maps with and without added noise.

1. Introduction. Let $\Omega \subset \mathbb{R}^2$ be the unit disk. Let $q = q_0 - E$ be the potential with the energy $E \in \mathbb{R}$, q_0 real-valued and $supp(q_0) \subset \Omega$. Consider the Schrödinger equation

$$(-\Delta + q)u = 0 \quad \text{in } \Omega \tag{1.1}$$

with the boundary condition $u = f$ on $\partial\Omega$. This boundary-value-problem might be well-posed; then for any $f \in H^{1/2}(\partial\Omega)$ it has a unique weak solution $u \in H^1(\Omega)$. For well-posed problems we define the Dirichlet-to-Neumann map (DN-map)

$$\Lambda_q : \quad H^{1/2}(\partial\Omega) \to H^{-1/2}(\partial\Omega), \quad f \mapsto \frac{\partial u}{\partial \nu}|_{\partial\Omega}, \tag{1.2}$$

where ν is the unit outer normal to the boundary. More precisely for $f, g \in H^{1/2}(\partial\Omega)$,

$$(\Lambda_q f, g)_{\partial\Omega} = \int_\Omega (\nabla u \cdot \nabla v + quv)dx, \tag{1.3}$$

where u is the unique weak solution for the boundary value f, and $v \in H^1(\Omega)$ with $v|_{\partial\Omega} = g$. The inverse problem of our interest is then the following; given Λ_q and the energy E, reconstruct the potential q_0. This is called the *Gel'fand-Dirichlet problem* first posed by Gel'fand [11].

The three novelties of this paper are:

1. We create a numerical algorithm for *Faddeev Green's function* for positive energy $E > 0$, a significant extension of the zero-energy case introduced in [30].
2. We propose a new numerical algorithm for reconstructing q_0 via the *D-bar method* when $E > 0$, it is then tested with radial and non-radial potentials using simulated data with noise.
3. We investigate numerically the *exceptional points* in which cases the aforementioned method fails, complementing the earlier work [23] focusing on the zero-energy case.

The D-bar method consists of exponentially behaving *Complex Geometrics Optics (CGO) solutions* first introduced by Faddeev [10], the *boundary integral equation* proved by R. G. Novikov [27], the *D-bar equation* discovered by Beals and Coifman [6], and finally the relation of the CGO solution and the potential by R. G. Novikov [26].

Electrical Impedance Tomography (EIT) and *Acoustic Tomography (AT)* are related to the Gel'fand-Dirichlet problem by a transformation resulting in different energies. We will see that EIT is a zero-energy problem with $E = 0$ and AT is a positive energy problem with $E > 0$.

We will identify the plane $\mathbb{R}^2$ as the complex plane by writing

$$z = [x_1 \ x_2]^T \in \mathbb{R}^2, \quad z = x_1 + \mathrm{i}x_2 \in \mathbb{C}.$$

*Department of Mathematics and Statistics, University of Helsinki, Finland.
†Department of Mathematics, Purdue University, West Lafayette IN 47907, USA
‡Department of Mathematics and Statistics, University of Helsinki, Finland.
§Department of Mathematics and Statistics, University of Helsinki, Finland.

1.1. Electrical Impedance Tomography. The inverse conductivity problem of Calderón [8] is the mathematical model of EIT. Let $\sigma : \Omega \to (0, \infty)$ be a bounded function satisfying $\sigma(z) \geq c > 0$. Let $v \in H^1(\Omega)$ be the unique solution to

$$\nabla \cdot \sigma \nabla v = 0 \text{ in } \Omega, \qquad v\big|_{\partial\Omega} = \phi. \tag{1.4}$$

Calderón's problem is to recover the electric conductivity distribution σ from the DN-map, or voltage-to-current map,

$$\Lambda_\sigma : \phi \mapsto \sigma \frac{\partial v}{\partial \nu}\Big|_{\partial\Omega}. \tag{1.5}$$

In EIT one attaches electrodes to the skin of a patient, feeds electric currents into the body and measures the resulting voltages at the electrodes. Repeating the measurement with several current patterns yields a current-to-voltage data matrix that can be used to compute an approximation to Λ_σ. Since different organs and tissues have different conductivities, recovering σ amounts to creating an image of the inner structure of the patient. This technique has commercial realizations, including breast cancer detection [1] and monitoring lung function[1]. See [22, 9] for more information on EIT and its applications.

Using the transformation $u = \sigma^{1/2} v$ we arrive at (1.1) with

$$q_0 = \sigma^{-1/2} \Delta \sigma^{1/2}, \quad E = 0.$$

Nachman gave a detailed proof of the D-bar method in [25] for solving σ in this EIT setting. The method was implemented numerically and tested with *in vivo* human data in [31, 21, 15, 16, 18, 22]. Furthermore, there are two similar EIT methods based on nonlinear frequency-domain techniques: [7], implemented in [17, 20, 14], and [4], implemented in [5, 3, 2, 22].

A crucial point of [25] is to prove that there are no exceptional points for *potentials of conductivity type*, defined as follows:

DEFINITION 1.1. *A compactly supported real-valued potential $q_0 \in C_0^\infty(\mathbb{R}^2)$ is of conductivity type if $q_0 = \phi^{-1}\Delta\phi$ for some real-valued $\phi \in C^\infty(\mathbb{R}^2)$ satisfying $\phi(z) \geq c > 0$ for all z in a bounded set $\Omega \subset \mathbb{R}^2$ and $\phi(z) = 1$ for all $z \in \mathbb{R}^2 \setminus \Omega$.*

1.2. Acoustic Tomography. We call the bounded function $\rho : \Omega \to (0, \infty)$ the *density* satisfying $\rho(x) \geq c > 0$. The *pressure* p satisfies the *reduced acoustic equation* for time-harmonic waves with frequency ω,

$$\nabla \cdot \left(\frac{1}{\rho} \nabla p\right) + \omega^2 \kappa p = 0 \quad \text{in } \Omega, \tag{1.6}$$

where $\kappa(z)$ is the compressibility and the speed of sound is given by $c(z) = (\kappa(z)\rho(z))^{-1/2}$. Given the boundary condition $p = f$ on $\partial\Omega$, the inverse problem of AT is to recover ρ and κ from the DN-map

$$\Lambda_{\omega,\kappa,\rho} : \quad f \to \frac{1}{\rho}\frac{\partial p}{\partial \nu}|_{\partial\Omega}. \tag{1.7}$$

Assuming $\rho|_{\partial\Omega} = \kappa|_{\partial\Omega} = 1$ and using the transformation $u = \rho^{-1/2} p$ we arrive at (1.1) with

$$q_0 = \rho^{1/2} \Delta \rho^{-1/2} - (\omega^2 \kappa \rho - E), \quad E = \omega^2 > 0. \tag{1.8}$$

As mentioned in [24] we have

$$\Lambda_q = \rho^{1/2} \Lambda_{\omega,\kappa,\rho} \rho^{1/2} - \frac{1}{2}\rho^{-1}\frac{\partial \rho}{\partial \nu},$$

so our assumptions imply $\Lambda_q = \Lambda_{\omega,\kappa,\rho}$.

As in the zero energy case of EIT, we have no exceptional points, as long as the potential q_0 is small enough compared to the energy. This notion will become clearer in the following sections.

[1] http://campaigns.draeger.com/pulmovista500/en/

1.3. Complex Geometrics Optics solutions and exceptional points. Rewrite (1.1) and consider special exponentially growing solutions $\psi(z,\zeta)$ of

$$(-\Delta + q_0)\psi(\cdot\,,\zeta) = E\psi(\cdot\,,\zeta) \quad \text{in } \mathbb{R}^2, \tag{1.9}$$

where q_0 is extended to the plane by zero and $\zeta = [\zeta_1\ \zeta_2]^T \in \mathbb{C}^2$ is a spectral parameter with $\Im(\zeta) \neq \mathbf{0}$. The exponential behaviour is then included in the requirement

$$\mathrm{e}^{-\mathrm{i}\zeta\cdot z}\psi(z,\zeta) - 1 \in X, \tag{1.10}$$

where X is some Banach space and $\zeta \cdot z = x_1\zeta_1 + x_2\zeta_2$.

If $\zeta \in \mathbb{R}^2$, we have a setting of a physical scattering of a particle with momentum ζ. If $\Im(\zeta) \neq \mathbf{0}$, we call the solutions $\psi(x,\zeta)$ *Complex Geometrics Optics* (CGO) solutions. For a given potential q_0 and parameter ζ there might not exist a unique CGO solution, then we call ζ an *exceptional point*. A more detailed definition is given later, based on the invertibility of the corresponding integral operator.

For large $|z|$ we can write $\exp(\mathrm{i}\zeta\cdot z)$ in place of $\psi(z,\zeta)$, and the equation (1.9) still has to hold, giving us

$$-\Delta \mathrm{e}^{\mathrm{i}\zeta\cdot z} = E\mathrm{e}^{\mathrm{i}\zeta\cdot z} \quad \Rightarrow \quad \zeta\cdot\zeta = E. \tag{1.11}$$

We can parametrize the subset of parameters ζ satisfying (1.11) by

$$\lambda = \frac{\zeta_1 + \mathrm{i}\zeta_2}{\sqrt{E}}, \quad \zeta = \begin{bmatrix} (\lambda + \frac{1}{\lambda})\frac{\sqrt{E}}{2} \\ (\frac{1}{\lambda} - \lambda)\frac{\mathrm{i}\sqrt{E}}{2} \end{bmatrix}. \tag{1.12}$$

We call the parameter λ also the spectral parameter. Let $\lambda = r\exp(\mathrm{i}\theta)$. Rewriting (1.12) gives

$$\zeta = \frac{\sqrt{E}}{2}\left((r + \frac{1}{r})\begin{bmatrix}\cos(\theta)\\ \sin(\theta)\end{bmatrix} + \mathrm{i}(r - \frac{1}{r})\begin{bmatrix}\sin(\theta)\\ -\cos(\theta)\end{bmatrix}\right). \tag{1.13}$$

Assuming $E > 0$, it is easy to see that $r \to 1$ implies $\Im(\zeta) \to \mathbf{0}$, meaning that the CGO solution goes to the limit of physical scattering. As the spectral parameter λ changes over the unit circle, the CGO solutions will have a jump. This leads to an additional term in the D-bar equation compared to the zero energy case.

We write

$$\mu(z,\zeta) = \mathrm{e}^{-\mathrm{i}\zeta\cdot z}\psi(z,\zeta)$$

and call it a CGO solution as well. Depending on whether we use ζ- or λ-notation, in place of $\psi(z,\zeta)$ and $\mu(z,\zeta)$ we write $\psi(z,\lambda)$ and $\mu(z,\lambda)$ respectively, even if the energy is then omitted; in the numerical part we only investigate the case $E = 1$.

The CGO solution $\mu(z,\zeta)$ satisfies another differential equation; starting from (1.9) we get

$$\begin{aligned} (-\Delta + q_0 - E)\mathrm{e}^{\mathrm{i}\zeta\cdot z}\mu(z,\zeta) &= 0 \\ \mathrm{e}^{\mathrm{i}\zeta\cdot z}(-\Delta - 2\mathrm{i}\zeta\cdot\nabla + \zeta\cdot\zeta + q_0 - E)\mu(z,\zeta) &= 0 \\ (L_\zeta + q_0)\mu(z,\zeta) &= 0, \end{aligned}$$

where

$$L_\zeta := -\Delta - 2\mathrm{i}\zeta\cdot\nabla.$$

The corresponding *Faddeev Green's function* $g_\zeta(z)$ satisfies

$$L_\zeta g_\zeta(z) = \delta_0. \tag{1.14}$$

In λ-notation we have

$$(L_\lambda + q_0)\mu(z,\lambda) = 0, \tag{1.15}$$

where

$$L_\lambda = -4\partial_z\bar{\partial}_z - 2\mathrm{i}\sqrt{E}(\lambda\partial_z + \frac{1}{\lambda}\bar{\partial}_z). \tag{1.16}$$

The Green's function of L_λ is denoted as $g_\lambda(z)$. Define the Lippman-Schwinger equation

$$\mu(z,\lambda) = 1 - g_\lambda(z) * (q_0(z)\mu(z,\lambda)). \tag{1.17}$$

If μ solves (1.17), then by applying the operator L_λ we see it also solves (1.15), so it is the CGO solution of our interest. Define the operators between suitable Banach-spaces X and Y,

$$\mathcal{Q} : X \to Y, \quad \mathcal{G}_\lambda : Y \to X,$$

by the equations

$$(\mathcal{Q}f)(z) = q_0(z)f(z), \tag{1.18}$$

$$(\mathcal{G}_\lambda f)(z) = g_\lambda(z) * f(z) = \int_{\mathbb{C}} g_\lambda(z - z')f(z')dz'. \tag{1.19}$$

Definition 1.2. *Let $\lambda \in \mathbb{C} \setminus \{0\}$ and $|\lambda| \neq 1$. The spectral parameter λ is an exceptional point, if $I + \mathcal{G}_\lambda\mathcal{Q}$ is not invertible.* If $\|\mathcal{G}_\lambda\mathcal{Q}\|_{\mathcal{L}(X)} < 1$, the operator $I + \mathcal{G}_\lambda\mathcal{Q}$ is invertible using the Neumann series and from (1.17) we can solve μ.

In future studies it would be preferable to define the spaces X and Y as Sobolev spaces in the spirit of Nachman's paper [25]. In the zero energy case, assuming the conductivity $\sigma \in W^{2,p}(\mathbb{R}^2), 1 < p < 2$ in (1.4), we have $X = W^{1,\tilde{p}}(\mathbb{R}^2), 1/\tilde{p} = 1/p - 1/2$ and $Y = L^p(\mathbb{R}^2)$. In the positive energy case the same approach to proving these inclusions does not work because of the extra term in the operator (1.16). Hopefully the computational study presented in this paper paves the way for further theoretical advances in this regard.

1.3.1. Absence of exceptional points for small potentials. We describe the proof of Proposition 4.1 in [28]. Let $E \in \mathbb{C}$, $\lambda \in \mathbb{C} \setminus \{0\}$, then proposition 3.1 in [28] states

$$|g_\lambda(z)| \leq \frac{\hat{c}}{\sqrt{|z|}\,|E|^{1/4}\sqrt{|\lambda| + 1/|\lambda|}}, \tag{1.20}$$

where

$$\hat{c} = \frac{1}{4}\max_{0<r<\infty}\left|\sqrt{r}Y_0(r)\right| + \frac{1}{4\pi}\max_{0<r<\infty,0\leq\phi_0\leq\pi}\left|\sqrt{r}\int_{\phi_0}^{\phi_0+\pi}\mathrm{e}^{\mathrm{i}r\sin\phi}d\phi\right|.$$

We assume $q_0(z)$ is smooth, real valued, and satisfies

$$\left|\partial_z^m\bar{\partial}_z^n q_0(z)\right| < \frac{C_{mn}}{(1+|z|)^{2+\varepsilon}}, \quad m,n \geq 0, \tag{1.21}$$

where C_{mn} and ε are positive constants. Related to this, we write

$$D_\epsilon = \int_{\mathbb{R}^2}\frac{1}{(1+|x|)^{2+\epsilon}}dx_1dx_2 = 2\pi\frac{1}{1+\epsilon}\frac{1}{\epsilon}.$$

Consider the operators $\mathcal{Q}$ and $\mathcal{G}_\lambda$ from (1.18) and (1.19) as

$$\begin{array}{rrcl} \mathcal{Q}: & C(\mathbb{R}^2) & \to & C(\mathbb{R}^2)\cap L^1(\mathbb{R}^2) \\ \mathcal{G}_\lambda: & C(\mathbb{R}^2)\cap L^1(\mathbb{R}^2) & \to & C(\mathbb{R}^2). \end{array}$$

We have

$$\|\mathcal{Q}(f)\|_{L^\infty(\mathbb{R}^2)} = \|q_0(z)f(z)\|_{L^\infty(\mathbb{R}^2)} \leq C_{00}\|f\|_{L^\infty(\mathbb{R}^2)},$$

and using (1.20)

$$\|\mathcal{G}_\lambda(f)\|_{L^\infty(\mathbb{R}^2)} \leq \frac{\hat{c}}{|E|^{1/4}\sqrt{|\lambda|+1/|\lambda|}}\left[\|f\|_{L^1} + \frac{4\pi}{3}\|f\|_{L^\infty(\mathbb{R}^2)}\right]. \tag{1.22}$$

We have

$$\begin{aligned}\|q_0 f\|_{L^1(\mathbb{R}^2)} &= \int_{\mathbb{C}} |q_0(z)f(z)|\,dz \leq \int_{\mathbb{C}} \frac{C_{00}|f(z)|}{(1+|z|)^{2+\epsilon}}dz \\ &\leq \int_{\mathbb{C}} \frac{C_{00}\|f\|_{L^\infty(\mathbb{R}^2)}}{(1+|z|)^{2+\epsilon}}dz = D_\epsilon C_{00}\|f\|_{L^\infty(\mathbb{R}^2)}.\end{aligned}$$

Thus

$$\begin{aligned}\|\mathcal{G}_\lambda(\mathcal{Q}f)\|_{\mathcal{L}^\infty(\mathbb{R}^2)} &\leq \frac{\hat{c}}{|E|^{1/4}\sqrt{|\lambda|+1/|\lambda|}}\left[\|Qf\|_{L^1(\mathbb{R}^2)} + \frac{4\pi}{3}\|Qf\|_{L^\infty(\mathbb{R}^2)}\right] \\ &\leq \frac{\hat{c}}{|E|^{1/4}}\left[D_\epsilon C_{00}\|f\|_{L^\infty(\mathbb{R}^2)} + \frac{4\pi}{3}C_{00}\|f\|_{L^\infty(\mathbb{R}^2)}\right] \\ &= \frac{C_{00}}{|E|^{1/4}}\hat{c}(D_\epsilon + \frac{4\pi}{3})\|f\|_{L^\infty(\mathbb{R}^2)}.\end{aligned}$$

Using the Neumann series this leads to the *norm smallness condition*

$$C_{00} < \frac{|E|^{1/4}}{\hat{c}(4\pi/3 + D_\epsilon)}, \tag{1.23}$$

giving us $\|\mathcal{G}_\lambda\mathcal{Q}\|_{\mathcal{L}(X)} < 1$ and unique solvability for μ. In other words, if the potential is small enough compared to the energy according to (1.23), there are no exceptional points. Also if the term $(|\lambda| + 1/|\lambda|)^{-1/2}$ is included, we have no exceptional points if $|\lambda|$ is large enough or close enough to zero.

1.4. The D-bar equation and the boundary integral equation. In this section we describe the D-bar method in more detail, all of the following is included in the survey [13] with different notation.

Define the differential operators

$$\begin{aligned}\partial_w &= \frac{1}{2}(\partial_{w_1} - \mathrm{i}\partial_{w_2}) \\ \bar{\partial}_w &= \frac{1}{2}(\partial_{w_1} + \mathrm{i}\partial_{w_2}),\end{aligned}$$

where $w = w_1 + \mathrm{i}w_2$. Define the exponential functions

$$e_{-\lambda}(z) := \exp\left(-\frac{\mathrm{i}\sqrt{E}}{2}(1+\mathrm{sgn}(E)\frac{1}{\lambda\overline{\lambda}})(\mathrm{sgn}(E)z\overline{\lambda} + \overline{z}\lambda)\right), \tag{1.24}$$

$$e_{\lambda}(z) := \exp\left(\frac{\mathrm{i}\sqrt{E}}{2}(1+\mathrm{sgn}(E)\frac{1}{\lambda\overline{\lambda}})(\mathrm{sgn}(E)z\overline{\lambda} + \overline{z}\lambda)\right). \tag{1.25}$$

Define the non-physical scattering transform by

$$\mathbf{t}(\lambda) = \int_{\mathbb{C}} e_\lambda(z)q_0(z)\mu(z,\lambda)dz, \tag{1.26}$$

Assume $|\lambda| \neq 1$. Then the following D-bar equation holds [12]:

$$\bar{\partial}_\lambda \mu(z,\lambda) = \operatorname{sgn}(|\lambda|^2 - 1)\frac{\mathbf{t}(\lambda)}{4\pi\overline{\lambda}} e_{-\lambda}(z)\overline{\mu(z,\lambda)}. \tag{1.27}$$

Define the operators

$$\mathcal{C}: \quad \mathcal{C}f(z,\lambda) = \frac{1}{\pi}\int_{\mathbb{C}} \frac{f(z,w)}{w-\lambda} dw, \tag{1.28}$$

$$\mathcal{T}: \quad \mathcal{T}f(z,\lambda) = \operatorname{sgn}(|\lambda|^2 - 1)\frac{\mathbf{t}(\lambda)}{4\pi\overline{\lambda}} e_{-\lambda}(z)\overline{f(z,\lambda)}, \tag{1.29}$$

$$\mathcal{M}: \quad \mathcal{M}f(z,\lambda) = \frac{1}{2\pi \mathrm{i}}\int_{|w|=1} \frac{f_+(z,w) - f_-(z,w)}{\lambda - w} \, |dw|\,, \tag{1.30}$$

where $f_\pm(z,\lambda)$ is the limit of $f(z,\lambda)$ when $|\lambda| \to 1^\pm$.

By applying the Cauchy-Green formula to (1.27) the CGO solution μ satisfies the integral equation

$$\mu(z,\lambda) = 1 - (\mathcal{C}\mathcal{T} - \mathcal{M})\mu(z,\lambda). \tag{1.31}$$

In the zero energy case we get similar integral equation where the operator $\mathcal{M}$ is absent.

Define the operator

$$(\mathcal{S}_\lambda \phi)(z) := \int_{\partial\Omega} G_\lambda(z-y)\phi(y) ds(y), \tag{1.32}$$

where

$$G_\lambda(z) = \mathrm{e}^{\frac{\mathrm{i}\sqrt{E}}{2}(\lambda\overline{z} + \frac{z}{\lambda})} g_\lambda(z).$$

The CGO solution $\psi(z,\lambda)$ satisfies the boundary integral equation [27]

$$(I + \mathcal{S}_\lambda(\Lambda_q - \Lambda_{-E}))\psi(\cdot,\lambda)|_{\partial\Omega} = \mathrm{e}^{\frac{\mathrm{i}\sqrt{E}}{2}(\lambda\overline{z} + \frac{1}{\lambda}z)}|_{\partial\Omega}, \tag{1.33}$$

where the DN-map Λ_{-E} corresponds to the potential $q_0 = 0$. In conjunction we have

$$\mathbf{t}(\lambda) = \int_{\partial\Omega} \mathrm{e}^{\frac{\mathrm{i}\sqrt{E}}{2}(\overline{\lambda}z + \overline{z}/\overline{\lambda})}(\Lambda_q - \Lambda_{-E})\psi(z,\lambda) dz. \tag{1.34}$$

The potential can be reconstructed by [26]

$$\mu(z,\lambda) = 1 + \frac{\mu_{-1}^\infty(z)}{\lambda} + \mathcal{O}(\frac{1}{\lambda}) \tag{1.35}$$

and

$$q_0(z) = 2\mathrm{i}\sqrt{E}\partial_z \mu_{-1}^\infty(z). \tag{1.36}$$

Thus we have the necessary steps to reconstruct the potential q_0 from the DN-map Λ_q, namely:

1. Solve $\psi(\cdot,\lambda)|_{\partial\Omega}$ from the boundary integral equation (1.33).
2. Compute the scattering transform using (1.34).
3. Choose a reconstruction point z' and solve $\mu(z',\lambda)$ from (1.31).
4. Compute $q_0(z')$ from (1.36).

In section 3 we give a more detailed numerical algorithm for this reconstruction procedure.

2. Simulation of measurement data. In this section we describe our method for simulating the measurement Λ_q on the unit disk. Choose an integer $N > 0$ and define a matrix $L_q : \mathbb{C}^{2N+1} \to \mathbb{C}^{2N+1}$ as follows. Use a truncated orthonormal trigonometric basis for representing functions defined at the boundary $\partial\Omega$:

$$\phi^{(n)}(\theta) = \frac{1}{\sqrt{2\pi}} \mathrm{e}^{\mathrm{i}n\theta}, \quad n = -N, ..., N. \tag{2.1}$$

Solve the problem

$$(-\Delta + q)u^{(n)} = 0 \text{ in } \Omega, \qquad u^{(n)} = \phi^{(n)} \text{ on } \partial\Omega \tag{2.2}$$

for $u^{(n)}$ using Finite Element Method. Define $L_q = [\widehat{u}(\ell, n)]$ by

$$\widehat{u}(\ell, n) = \int_{\partial\Omega} \frac{\partial u^{(n)}}{\partial \nu} \overline{\phi^{(\ell)}} ds. \tag{2.3}$$

Here ℓ is the row index and n is the column index. The integration can be computed when the set $[0, 2\pi)$ is divided into discrete points. The matrix L_q represents the operator Λ_q of (1.2) approximately.

We add simulated measurement noise by defining

$$L_q^\epsilon := L_q + cG, \tag{2.4}$$

where G is a $(2N + 1) \times (2N + 1)$ matrix with random entries independently distributed according to the Gaussian normal density $\mathcal{N}(0, 1)$. The constant $c > 0$ can be adjusted for different relative errors $\|L_q^\epsilon - L_q\| / \|L_q\|$, where $\|\cdot\|$ is the standard matrix norm.

The DN-map Λ_{-E} is represented by the matrix L_{-E} in a similar way, in the boundary value problem (2.2) we then have $q = -E$.

3. Numerical implementation of the D-bar method. Choose an integer $N_\lambda > 0$ and radii $1 < R_1 < R_2$. For spectral parameters $R_1 < |\lambda| < R_2$ define a $N_\lambda \times N_\lambda$ grid. The radius $R_1 > 1$ is taking out values of λ close to the unit circle, since we have problems in computing the Faddeev Green's function for these values, as will be seen. The radius R_2 is analog to the truncation radius of the zero-energy case acting as a regulation parameter. The larger $|\lambda|$ will result in computational problems, which can be seen from the computed scattering transform.

It turns out we might have a non-symmetric area of usable scattering data in the spectral parameter space, in contrast to the zero energy case. We put the scattering transform to zero outside of an ellipse, whose radius in polar coordinates is

$$r(\theta) = \frac{\sqrt{2}ab}{\sqrt{(b^2 - a^2)\cos(2\theta - 2\phi) + a^2 + b^2}}, \tag{3.1}$$

where a and b are the semidiameters and the ellipse is rotated by ϕ.

3.1. Solving the boundary integral equation. Fix $N_\lambda = 256$, $R_1 = 1.01$ and $R_2 = 15$. For any λ in the grid we compute the matrix representation $S_\lambda = [\widehat{s}(\ell, n)]$ of the operator $\mathcal{S}_\lambda$ (1.32) defined by

$$\widehat{s}(\ell, n) = \int_{\partial\Omega} s^{(n)} \overline{\phi^{(\ell)}} ds, \quad s^{(n)} = \int_{\partial\Omega} G_\lambda(z - y)\phi^{(n)}(y) ds(y). \tag{3.2}$$

Again ℓ is the row index and n is the column index, and the set $[0, 2\pi)$ is divided into discrete points. The functions $\psi(z, \lambda)|_{\partial\Omega}$ and $\exp(\mathrm{i}\sqrt{E}/2(\lambda\overline{z} + z/\lambda))|_{\partial\Omega}$ can be expressed as vectors $\psi_\lambda^{\mathrm{vec}}$ and e_λ^{vec}, respectively, using the basis functions $\phi^{(n)}$. Then, the boundary integral equation (1.33) is approximated by the equation

$$(\mathrm{I} + S_\lambda(L_q - L_{-E}))\psi_\lambda^{\mathrm{vec}} = e_\lambda^{\mathrm{vec}}, \tag{3.3}$$

where I is the correct sized unit matrix. This is easily solved for the vector $\psi_\lambda^{\text{vec}}$ by inverting the matrix $\mathrm{I} + S_\lambda(L_q - L_{-E})$.

In computing the matrix S_λ we need a computational method for the Faddeev Green's function $g_\lambda(z)$. This non-trivial method is described in detail in section 4.

3.2. Computing the truncated scattering transform. We use the basis functions to change the vector $(L_q - L_{-E})\psi_\lambda^{\text{vec}}$ into its function representation, after which we simply use (1.34) to get $\mathbf{t}(\lambda)$ for any λ in the grid.

For any potential (small enough so that there are no exceptional points) we have the symmetry

$$\mathbf{t}(1/\overline{\lambda}) = \mathbf{t}(\lambda).$$

Using this symmetry we can construct the scattering transform inside the unit circle. Depending on the scattering transform, choose the parameters a, b, ϕ for the ellipse (3.1) inside of which the numerical computation is usable. Use the truncated scattering transform

$$\mathbf{t}_R(\lambda) = \begin{cases} 0, & |\lambda| \le 1/r(\theta) \\ \mathbf{t}(1/\overline{\lambda}), & 1/r(\theta) \le |\lambda| < 1/R_1 \\ 0, & 1/R_1 \le |\lambda| \le R_1 \\ \mathbf{t}(\lambda), & R_1 < |\lambda| < r(\theta) \\ 0, & |\lambda| \ge r(\theta). \end{cases}$$

3.3. Solving the integral equation. We can solve the periodic version of the integral equation (1.31) using $\mathbf{t}_R$ and the analog of the solver fully detailed in [19]. The difference to the traditional method is the operator $\mathcal{M}$ which is implemented the following way. We approximate $\mathcal{M}$ by the operator $\mathcal{M}_\epsilon$ defined by

$$\mathcal{M}_\epsilon f(z,\lambda) = \frac{1}{2\mathrm{i}\pi} \int_{|w|=1} \frac{f_\epsilon(z,w) - f_{-\epsilon}(z,w)}{\lambda - w} \, |dw| \,, \tag{3.4}$$

where $f_\epsilon(z,w) = f(z,w)|_{|z|=1+\epsilon}$. For the integration we divide the set $[0, 2\pi)$ into 128 discrete points. During the iteration for solving the periodic solution $\mu_R(z,\lambda)$ we interpolate the intermediate solution $\mu_R'(z,\lambda)$ at the points $(1+\epsilon)\exp(\mathrm{i}\theta)$ and $(1-\epsilon)\exp(\mathrm{i}\theta)$ to get the functions $\mu_{R,\epsilon}'(z,\lambda)$ and $\mu_{R,-\epsilon}'(z,\lambda)$ respectively. Thus the integration in (3.4) can be done and the effect of the operator $\mathcal{M}_\epsilon$ is added to the process.

Note that at the moment we do not have an analytical proof for the existence of the periodic solution $\mu_R(z,\lambda)$, nor that it converges to the original CGO solution $\mu(z,\lambda)$, nor any error estimates; however the results of the numerical tests of section 5 suggest that we can prove these things after suitable Sobolev spaces X, Y of section 1.3 have been established; the solution μ_R is always found and it seems to be correct as the reconstructions are correct.

3.4. Reconstructing the potential. Let z_r be the reconstruction point of our choosing. Let dz be the finite difference and define the points $z_1 = z_r + dz$, $z_2 = z_r - dz$, $z_3 = z_r + \mathrm{i}\cdot dz$, $z_4 = z_r - \mathrm{i}\cdot dz$. Using the earlier described methods we can solve the corresponding CGO solutions $\mu_R^i = \mu_R(z_i, \lambda)$, $i = 1, 2, 3, 4$. We combine the equations (1.35) and (1.36), omit the term $\mathcal{O}(1/\lambda)$, use a finite λ and finite difference method for the differentiation to get the approximate reconstruction equation

$$q_0(z_r) \approx \lambda \left(\frac{\mu_R^2 - \mu_R^1}{2dz} + \mathrm{i}\frac{\mu_R^3 - \mu_R^4}{2dz} \right). \tag{3.5}$$

Note that the result is computed in a grid of parameters λ; we take the average value over the indices for which $|\lambda| \approx a$, since these are largest available.

4. Computation of the Faddeev Green's function for positive energy. We need a numerical algorithm for $g_\lambda(z)$ for any λ, $|\lambda| > 1$ and any point $z \in D(0,1)$. We look at the Faddeev Green's function with regards to the parameter ζ to see useful relations. In the case $\zeta \cdot \zeta = E = 0$ and $\zeta^I \neq \mathbf{0}$ the numerical computation of $g_\zeta(z)$ is presented in [30]. We extend the method for $\zeta \cdot \zeta = E > 0$.

Using the Fourier transform, starting from (1.14), we have

$$\begin{aligned}(-\triangle - 2\mathrm{i}\zeta\cdot\nabla)g_\zeta &= \delta_0\\ \mathcal{F}((-\tfrac{\partial^2}{\partial {x_1}^2} - \tfrac{\partial^2}{\partial {x_2}^2} - 2\mathrm{i}\zeta_1\tfrac{\partial}{\partial x_1} - 2\mathrm{i}\zeta_2\tfrac{\partial}{\partial x_2})g_\zeta) &= \mathcal{F}(\delta)\\ (-(\mathrm{i}y_1)^2 - (\mathrm{i}y_2)^2 - 2\mathrm{i}\zeta_1(\mathrm{i}y_1) - 2\mathrm{i}\zeta_2(\mathrm{i}y_2))\hat{g}_\zeta(y) &= 1/(2\pi)\\ (y\cdot y + 2\zeta\cdot y)\hat{g}_\zeta(y) &= 1/(2\pi)\end{aligned}$$

Using the inverse Fourier transform we get

$$g_\zeta(z) = \frac{1}{(2\pi)^2}\int_{\mathbb{R}^2}\frac{\mathrm{e}^{\mathrm{i}y\cdot z}}{y\cdot y + 2\zeta\cdot y}dy. \tag{4.1}$$

The following relations can be seen from (4.1).

LEMMA 4.1. *Let $\alpha \in \mathbb{R}\setminus\{0\}$, R a rotational matrix with $\det(R) = 1$ and $R\zeta = R\zeta^R + iR\zeta^I$. Then the Faddeev Green's function $g_\zeta(z)$ satisfies*

$$g_\zeta(\alpha z) = g_{\alpha\zeta}(z) \tag{4.2}$$

$$g_\zeta(Rz) = g_{R^{-1}\zeta}(z) \tag{4.3}$$

$$g_\zeta\left(\begin{bmatrix}-x_1\\ x_2\end{bmatrix}\right) = g_{\begin{bmatrix}-\zeta_1\\ \zeta_2\end{bmatrix}}(z) \tag{4.4}$$

$$g_\zeta\left(\begin{bmatrix}x_1\\ -x_2\end{bmatrix}\right) = g_{\begin{bmatrix}\zeta_1\\ -\zeta_2\end{bmatrix}}(z) \tag{4.5}$$

$$g_{\overline{\zeta}}(z) = \overline{g_\zeta(-z)}. \tag{4.6}$$

Using relations (4.6) and (4.5) we have

$$\overline{g_\zeta(-z)} = g_{\overline{\zeta}}(z) = g_\zeta\left(\begin{bmatrix}x_1\\ -x_2\end{bmatrix}\right),$$

which results to a switching relation

$$g_\zeta\left(\begin{bmatrix}-x_1\\ x_2\end{bmatrix}\right) = \overline{g_\zeta\left(\begin{bmatrix}x_1\\ x_2\end{bmatrix}\right)} \tag{4.7}$$

We can use the rotation relation (4.3) to reduce ζ to the form

$$\zeta = \begin{bmatrix}k_1\\ 0\end{bmatrix} + \mathrm{i}\begin{bmatrix}0\\ k_2\end{bmatrix}, \quad |k_1| > k_2 > 0. \tag{4.8}$$

The strategy for computing $g_\lambda(z)$ is now the following:

1. Use (1.12) to compute ζ from λ.
2. Find the rotational matrix R that satisfies $R\zeta_I = [0, k_2]^T$ for some $k_2 > 0$; then write

$$g_\zeta(z) = g_{R^{-1}R\zeta}(z) = g_{R\zeta}(Rz),$$

where $R\zeta$ is in the reduced form (4.8).

3. For very small $|z|$ use a method of single layer potential described in section 4.4.
4. Use relation (4.2) to scale points outwards (since small $|z|$ are a problem as will be seen later) and relation (4.7) to switch from $x_1 < 0$ to $x_1 \geq 0$.
5. Use computational domains to compute $g_\zeta(z)$ for reduced ζ and z with $x_1 \geq 0$.

It takes some analysis to find suitable computational domains for the last step.

4.1. Analytical integration, part one. Assume we have the reduced ζ of (4.8) and the switched $z = x_1 + \mathrm{i}x_2$ with $x_1 \geq 0$. Write $t = y_1 + k_1$, $a = (y_2 + k_2\mathrm{i})^2 - E$ and subsequently the denominator of the integrand in (4.1) as

$$\begin{aligned} y \cdot y + 2y \cdot \zeta &= y_1^2 + y_2^2 + 2y_1k_1 + 2y_2k_2\mathrm{i} \\ &= (y_1 + k_1)^2 + (y_2 + k_2\mathrm{i})^2 - E \\ &= t^2 + a \\ &= (t + \mathrm{i}\sqrt{a})(t - \mathrm{i}\sqrt{a}) \end{aligned}$$

We define the square root in the same way MATLAB calculates it by default, that is for a complex number $z = r\exp(\mathrm{i}\theta), 0 \leq \theta < 2\pi, r \geq 0$ the square root is

$$\sqrt{z} = \begin{cases} \sqrt{r}\mathrm{e}^{\mathrm{i}\theta/2} & , \quad 0 \leq \theta \leq \pi, \\ \sqrt{r}\mathrm{e}^{-\mathrm{i}(2\pi-\theta)/2} & , \quad \pi < \theta < 2\pi. \end{cases}$$

This way the square root has the following properties: for any $z \in \mathbb{C}$ we have

$$\Re(\sqrt{z}) \geq 0 \tag{4.9}$$

$$\sqrt{\overline{z}} = \overline{\sqrt{z}}. \tag{4.10}$$

The numerator of the integrand in (4.1) numerator becomes

$$\begin{aligned} \mathrm{e}^{\mathrm{i}z\cdot y} &= \mathrm{e}^{\mathrm{i}(x_1(t-k_1)+x_2y_2)} \\ &= \mathrm{e}^{\mathrm{i}(x_2y_2-x_1k_1)}\mathrm{e}^{\mathrm{i}x_1t}. \end{aligned}$$

The integral in (4.1) is thus transformed into

$$\int_{\mathbb{R}^2} \frac{\mathrm{e}^{\mathrm{i}y\cdot z}}{y \cdot y + 2\zeta \cdot y} d\mathbf{y} = \int_{-\infty}^{\infty} \mathrm{e}^{\mathrm{i}(x_2y_2-x_1k_1)} \left(\int_{-\infty}^{\infty} \frac{\mathrm{e}^{\mathrm{i}x_1t}}{(t + \mathrm{i}\sqrt{a})(t - \mathrm{i}\sqrt{a})} dt \right) dy_2.$$

The integral over the real parameter t is complexified with $w = w_R + \mathrm{i}w_I \in \mathbb{C}$ and we write

$$f(w) = \frac{\mathrm{e}^{\mathrm{i}x_1w}}{(w + \mathrm{i}\sqrt{a})(w - \mathrm{i}\sqrt{a})} = \frac{\mathrm{e}^{\mathrm{i}x_1w_R}\mathrm{e}^{-x_1w_I}}{(w + \mathrm{i}\sqrt{a})(w - \mathrm{i}\sqrt{a})}, \tag{4.11}$$

The poles of the function $f(w)$ are $\pm\mathrm{i}\sqrt{a}$, where

$$a = (y_2 + k_2\mathrm{i})^2 - E = y_2^2 - E - k_2^2 + 2y_2k_2\mathrm{i}.$$

It follows from our definition of $\sqrt{\cdot}$ that

- when $y_2 > 0$, a is in the upper half plane, so $\mathrm{i}\sqrt{a}$ is in quadrant 2 and $-\mathrm{i}\sqrt{a}$ in quadrant 4 (note, that $k_2 > 0$), and
- when $y_2 < 0$, a is in the lower half plane, so $\mathrm{i}\sqrt{a}$ is in quadrant 1 and $-\mathrm{i}\sqrt{a}$ in quadrant 3.

When $w_I, x_1 \geq 0$ we have

$$|f(w)| \to 0, \quad \text{as } |w| \to \infty.$$

We choose the integration path

$$\Gamma = [-R, R] \cup \{w | w = R\exp(\mathrm{i}\theta), 0 \leq \theta \leq \pi\},$$

so when $R \to \infty$ the pole $w = \mathrm{i}\sqrt{a}$ is inside the path. Using Residue calculus we get

$$\begin{aligned}\int_{\mathbb{R}\subset\mathbb{C}} f(w)dw = \int_{\Gamma} f(w)dw &= 2\pi\mathrm{i} \operatorname*{Res}_{w=\mathrm{i}\sqrt{a}} f(w) \\ &= 2\pi\mathrm{i} \lim_{w\to\mathrm{i}\sqrt{a}} (w-\mathrm{i}\sqrt{a}) f(w) = 2\pi\mathrm{i}\frac{\mathrm{e}^{\mathrm{i}x_1(\mathrm{i}\sqrt{a})}}{\mathrm{i}\sqrt{a}+\mathrm{i}\sqrt{a}} \\ &= \pi\frac{\mathrm{e}^{-x_1\sqrt{a}}}{\sqrt{a}}\end{aligned}$$

Thus

$$\begin{aligned}g_\zeta(z) &= \frac{1}{(2\pi)^2}\left(\int_{-\infty}^{0} \mathrm{e}^{\mathrm{i}(x_2y_2-x_1k_1)}\pi\frac{\mathrm{e}^{-x_1\sqrt{a}}}{\sqrt{a}}dy_2 + \int_0^{\infty} \mathrm{e}^{\mathrm{i}(x_2y_2-x_1k_1)}\pi\frac{\mathrm{e}^{-x_1\sqrt{a}}}{\sqrt{a}}dy_2\right) \\ &= \frac{1}{4\pi}\mathrm{e}^{-\mathrm{i}x_1k_1}\left(\int_0^{\infty} \mathrm{e}^{-\mathrm{i}x_2y_2}\frac{\mathrm{e}^{-x_1\sqrt{\bar{a}}}}{\sqrt{\bar{a}}}dy_2 + \int_0^{\infty} \mathrm{e}^{\mathrm{i}x_2y_2}\frac{\mathrm{e}^{-x_1\sqrt{a}}}{\sqrt{a}}dy_2\right).\end{aligned}$$

Because of (4.9) we have

$$\mathrm{e}^{-\mathrm{i}x_2y_2}\frac{\mathrm{e}^{-x_1\sqrt{\bar{a}}}}{\sqrt{\bar{a}}} = \overline{\mathrm{e}^{\mathrm{i}x_2y_2}\frac{\mathrm{e}^{-x_1\sqrt{a}}}{\sqrt{a}}},$$

and so

$$g_\zeta(z) = \frac{1}{2\pi}\mathrm{e}^{-\mathrm{i}x_1k_1}\Re\left(\int_0^{\infty} \mathrm{e}^{\mathrm{i}x_2t}\frac{\mathrm{e}^{-x_1\sqrt{a}}}{\sqrt{a}}dt\right), \quad x_1 \geq 0, \tag{4.12}$$

where $a = (t+k_2\mathrm{i})^2 - E$ and we have changed the symbol y_2 to t.

4.1.1. Observations. The starting point in our numerical experiments is the parameter λ with $|\lambda| > 1$. Using (1.12) we can see, that as $|\lambda| \to 1$ we have $k_2 \to 0$. When $|\lambda| \to \infty$, we have $|k_1|, k_2 \to \infty$.

We want to numerically compute the integral of (4.12). We can only compute up to a finite limit, say from 0 to N. Two problems might occur, the integrand either converges slowly, meaning we have to take N very large, or the integrand might oscillate fast, meaning we have to take a great number of integration points in $[0, N]$.

Taking these considerations into account, we see that problematic situations in using (4.12) arise when x_2 is large (oscillation), x_1 is small (convergence) and when k_2 is large (oscillation). When x_1 is large we have oscillation, but also better convergence. When λ is close to one, then k_2 is close to zero and the poles $\pm i\sqrt{a}$ are close to the integration path Γ causing numerical problems.

This leads to the following enhancements. The different computational domains will use different versions of (4.12).

4.2. Analytical integration, part two. Write

$$g(w) = \mathrm{e}^{\mathrm{i}x_2w}\frac{\mathrm{e}^{-x_1\sqrt{a}}}{\sqrt{a}}, \quad a = (w+k_2\mathrm{i})^2 - E, \quad w = w_1 + \mathrm{i}w_2 \in \mathbb{C},$$

and consider the complexified integral $\int_{\mathbb{R}^+} g(w)dw$ of (4.12). We have

$$\mathrm{e}^{\mathrm{i}x_2w} = \mathrm{e}^{\mathrm{i}x_2w_1}\mathrm{e}^{-x_2w_2},$$

so when $x_2, w_2 \geq 0$ or $x_2, w_2 < 0$ we have

$$|g(w)| \to 0 \text{ as } |w| \to \infty. \tag{4.13}$$

Note that the numerator $\exp(-x_1\sqrt{a})$ converges, since $x_1 \geq 0$ and (4.9) holds. The branch points of $g(w)$ are $\pm\sqrt{E} - k_2\mathrm{i}$.

4.2.1. The case $x_2 \geq 0$. We choose the integration path

$$\Gamma_1 = [0, R] \cup \{w | w = R\exp(\mathrm{i}\theta), 0 \leq \theta \leq \pi/2\} \cup \{\mathrm{i}R(1-t), \quad 0 \leq t \leq 1\}.$$

We have $\int_{\Gamma_1} g(w)dw = 0$, since $g(w)$ is analytic in the first quadrant. Because of (4.13) we then have

$$\int_{\mathbb{R}^+} g(w)dw = -\int_{\infty}^{0} g(\mathrm{i}t)\mathrm{i}dt = \int_0^{\infty} \mathrm{e}^{-x_2 t} \frac{\mathrm{e}^{-x_1 \mathrm{i}\sqrt{(t+k_2)^2+E}}}{\sqrt{(t+k_2)^2+E}} dt,$$

and so

$$= \frac{1}{2\pi} \mathrm{e}^{-\mathrm{i}x_1 k_1} \Re \left(\int_0^{\infty} \mathrm{e}^{-x_2 t} \frac{\mathrm{e}^{-x_1 \mathrm{i}\sqrt{t^2+k_1^2+2tk_2}}}{\sqrt{t^2+k_1^2+2tk_2}} dt \right). \tag{4.14}$$

The integrand in (4.14) converges quickly for large x_2 and has high oscillation for large x_1.

4.2.2. The case $x_2 < 0$. The branch point $\sqrt{E} - k_2\mathrm{i}$ is avoided by integrating along

$$\begin{aligned} \Gamma_2 \; &= \; [0, \sqrt{E}+1] \cup (\{-\mathrm{i}Rt : 0 \leq t \leq 1\} \cup \{w = R\exp(\mathrm{i}\theta) : \frac{3}{2}\pi \leq \theta \leq 2\pi\} \\ &\quad \cup \{(\sqrt{E}+1)t + (1-t)R : 0 \leq t \leq 1\}) \\ &:= P_1 \cup (L_1 \cup L_2 \cup L_3), \end{aligned}$$

where $g(w)$ is analytical inside the loop $L_1 \cup L_2 \cup L_3$, and $|g(w)| \to 0$ on the circle L_2 as $R \to \infty$. Thus

$$\int_{\mathbb{R}^+} g(w)dw = I_1 + \int_0^{\infty} g(\sqrt{E}+1-\mathrm{i}t)(-\mathrm{i})dt,$$

where

$$\begin{aligned} I_1 &= \textstyle\int_0^{\sqrt{E}+1} g(t)dt \\ \textstyle\int_0^{\infty} g(\sqrt{E}+1-\mathrm{i}t)(-\mathrm{i})dt &= \textstyle\int_0^{\infty} \mathrm{e}^{\mathrm{i}(\sqrt{E}+1)x_2} \mathrm{e}^{x_2 t} \frac{\mathrm{e}^{-x_1\sqrt{b}}}{\sqrt{b}} (-\mathrm{i})dt, \end{aligned}$$

and $b = (\sqrt{E}+1+(k_2-t)\mathrm{i})^2 - E$. In total

$$g_\zeta(z) = \frac{1}{2\pi} \mathrm{e}^{-\mathrm{i}x_1 k_1} \Re \left(I_1 - \mathrm{i}\mathrm{e}^{\mathrm{i}(\sqrt{E}+1)x_2} \int_0^{\infty} \mathrm{e}^{x_2 t} \frac{\mathrm{e}^{-x_1\sqrt{b}}}{\sqrt{b}} dt \right) \tag{4.15}$$

The integrand in (4.15) converges quickly for large $|x_2|$ and has high oscillation for large x_1.

4.3. Choosing upper limits for the integrals. Write $g_\zeta^{T_1}$,$g_\zeta^{T_2}$ and $g_\zeta^{T_3}$ for the finite integrals for (4.12),(4.14) and (4.15) respectively. We need to choose the upper limits T_i, $i = 1, 2, 3$. There will be numerical error caused by the neglected part of the integral and the numerical integration method used. It is decided to simply require

$$\left| g_\zeta - g_\zeta^{T_x i} \right| < 1E-8. \tag{4.16}$$

The error caused by the numerical integration method is assumed to be not dependant on λ or z. For $g_\zeta^{T_i}$, the integration range $[0, T_i]$ is divided into M_i points (with $g_\zeta^{T_3}$ there is also the additional integral I_1) and the Gaussian quadrature is used. The integers M_i are chosen large enough so that for any integer $M > M_i$ the first 8 digits are not changing in the numerical value of $g_\zeta^{T_i}(z)$. In this test the choice of z has only a minor effect, it is done by choosing the "worst" possible point for

any given computational domain; for example, for $g_\zeta^{T_1}(z)$ using $z = [1, 1]$ the integrand has more oscillation than with the point $z = [1, 0]$, and thus needs a larger parameter M_1.

Finding T_i is a bit cumbersome and is explained in the following. In (4.12) we have the term a and

$$\begin{aligned}|\sqrt{a}| &= \left|\sqrt{(t^2 - k_2^2 - E) + 2k_2 t\mathrm{i}}\right| = ((t^2 - k_1^2)^2 + 4k_2^2 t^2)^{1/4} \\ &= (t^4 - 2t^2k_1^2 + k_1^4 + 4k_2^2t^2)^{1/4} \\ &\geq (t^4 - 2k_1^2t^2)^{1/4} \geq (t^4 - 1/2t^4)^{1/4} \\ &= \frac{t}{2^{1/4}}, \end{aligned} \tag{4.17}$$

when $t \geq 2\,|k_1|$. Then, writing θ for the angle $\sqrt{a} = r\exp(\mathrm{i}\theta)$,

$$\begin{aligned}\left|\frac{\mathrm{e}^{-x_1\sqrt{a}}}{\sqrt{a}}\right| &\leq \frac{\mathrm{e}^{-x_1\Re(\sqrt{a})}}{t/2^{1/4}} = \frac{\mathrm{e}^{-x_1\cos(\theta)|\sqrt{a}|}}{t/2^{1/4}} \\ &\leq \frac{\mathrm{e}^{-x_1\cos(\theta)t/2^{1/4}}}{t/2^{1/4}}.\end{aligned}$$

The angle goes to zero as $t \to \infty$, so $\cos(\theta) \to 1^-$. Since $t \geq 2\,|k_1|$ we write $c_1 = \cos(\theta_1)$, where the angle of $\sqrt{a}|_{t=2k_1}$ is θ_1, and so we have for the integral

$$\begin{aligned}\left|\int_T^\infty \mathrm{e}^{\mathrm{i}x_2 t}\frac{\mathrm{e}^{-x_1\sqrt{a}}}{\sqrt{a}}dt\right| &\leq \int_T^\infty \frac{\mathrm{e}^{-x_1c_1t/2^{1/4}}}{t/2^{1/4}}dt \\ &= 2^{1/4}\int_{x_1c_1T/2^{1/4}}^\infty \frac{\mathrm{e}^{-s}}{s}ds = 2^{1/4}E_i(x_1c_1T/2^{1/4}).\end{aligned} \tag{4.18}$$

The exponential integral function E_i can be computed in MATLAB with *expint.m*. Because of (4.16) we require that the remainder (4.18) is of the order $2\pi/2^{1/4} \cdot 1E-8 \approx 7.47E-8$. We can test with MATLAB that $E_i(14) < 6E-8$, so we get

$$\begin{aligned}x_1c_1T/2^{1/4} &= 14 \\ T &= \tfrac{14\cdot 2^{1/4}}{x_1c_1}.\end{aligned}$$

Finally,

$$T_1 = \max\{\frac{14\cdot 2^{1/4}}{x_1c_1}, 2k_1\}. \tag{4.19}$$

From (4.14) we easily get

$$\begin{aligned}\left|\int_{T_2}^\infty \mathrm{e}^{-x_2t}\frac{\mathrm{e}^{-x_1\mathrm{i}\sqrt{t^2+k_1^2+2tk_2}}}{\sqrt{t^2+k_1^2+2tk_2}}dt\right| &\leq \int_{T_2}^\infty \frac{\mathrm{e}^{-x_2t}}{t}dt \\ &= E_i(x_2T_2).\end{aligned}$$

Thus the upper limit can be computed, as before, from

$$\begin{aligned}x_2T_2 &= 14 \\ T_2 &= \frac{14}{x_2}.\end{aligned} \tag{4.20}$$

Starting from (4.15) we have

$$\begin{aligned}\left|\sqrt{b}\right| &= ((k_2-t)^4 + 2(2\sqrt{E}+1)(k_2-t)^2 + (2\sqrt{E}+1)^2 \\ &\quad +4(\sqrt{E}+1)^2(k_2-t)^2)^{1/4} \\ &\geq ((k_2-t)^4)^{1/4} = |t-k_2|\,.\end{aligned}$$

Using the same argument as preceding (4.18), we write $c_2 = \cos(\theta_2)$, where the angle of $\sqrt{b}|_{t=k_2}$ is θ_2. Then for $T_2 > k_2$ we have

$$\begin{aligned}\left|\int_{T_3}^{\infty} \mathrm{e}^{x_2 t}\frac{\mathrm{e}^{-x_1\sqrt{b}}}{\sqrt{b}}dt\right| &\leq \int_{T_3}^{\infty}\frac{\mathrm{e}^{x_2 t - x_1 c_2(t-k_2)}}{t-k_2}dt \\ &= \mathrm{e}^{x_2 k_2}\int_{(c_2x_1-x_2)(T_3-k_2)}^{\infty}\frac{\mathrm{e}^{-s}}{s}ds \\ &= \mathrm{e}^{x_2 k_2}E_i((c_2x_1-x_2)(T_3-k_2)) \\ &\leq E_i((c_2x_1-x_2)(T_3-k_2)).\end{aligned}$$

As before,

$$\begin{aligned}(c_2x_1-x_2)(T_3-k_2) &= 14 \\ T_3 &= \frac{14}{c_2x_1-x_2}+k_2.\end{aligned} \tag{4.21}$$

The use of these choices of upper limits guarantees us

$$\left|g_\zeta(z) - g_\zeta^{T_i}(z)\right| < 1E-8, \quad i=1,2,3.$$

4.4. Use of single-layer potential for small z. For small values of z there is a problem of slow convergence. We will evade this problem by the use of the single-layer potential for a function that satisfies the Helmholtz equation.

Write

$$E = k^2, \quad G_\zeta(z) = \exp(\mathrm{i}\zeta\cdot z)g_\zeta(z), \quad G(z) = \mathrm{i}H_0^1(k\,|z|)/4,$$

where H_0^1 is Hankel's function of the first type. We have

$$\begin{aligned}(-\triangle - k^2)G_\zeta(z) &= \delta_z \\ (-\triangle - k^2)G(z) &= \delta_z,\end{aligned}$$

so

$$(-\triangle - k^2)(G_\zeta - G) = 0.$$

Write $H_\zeta := G_\zeta - G$. For any radius R there exists a single-layer potential $p(z)$, which gives the value of H_ζ by the integral

$$H_\zeta(z) = \int_{\partial D(0,R)}\frac{\mathrm{i}}{4}H_0^1(k\,|z-y|)p(y)d\mu(y) := S(p(\cdot))(z). \tag{4.22}$$

Assume we know $H_\zeta(z)$ on the circle $\partial D(0,R)$, where R is large enough so that we don't have the problems of slow convergence. The potential can be recovered by the inverse of the integral operator, $p = S^{-1}(H_\zeta(z))$. Then $H_\zeta(z)$ can be calculated using (4.22) for any $|x| < R$. Finally we have

$$g_\zeta(z) = \mathrm{e}^{-\mathrm{i}\zeta\cdot z}(H_\zeta(z) + G(z)). \tag{4.23}$$

More detailed description of this submethod is given in section 4.5.1

4.5. Computational domains and the computation of $g_\zeta(z)$. The plane $\mathbb{R}^2$ is divided into computational domains as shown in Figure 1. The disks shown are $D_1 = D(0, 0.2)$, $D_2 = D(0, 0.5)$, $D_3 = D(0, 1)$, and not in scale is pictured $D_4 = D(0, 2.5)$. Domain 1a is the disk D_1, domain 1b is the annulus $D_2 \setminus D_1$, domain 1c is the annulus $D_3 \setminus D_2$. Domains 2,3,4,5,6 and 7 form the annulus $D_4 \setminus D_3$.

Domains 2 and 3 are divided by the line $x_2 = 0.5x_1$, domains 3 and 4 by $x_1 = 0$, domains 4 and 5 by $x_2 = -0.5x_1$, domains 5 and 6 by $x_2 = 0.5x_1$, domains 6 and 7 by $x_1 = 0$ and finally domains 7 and 2 by $x_2 = -0.5x_1$.

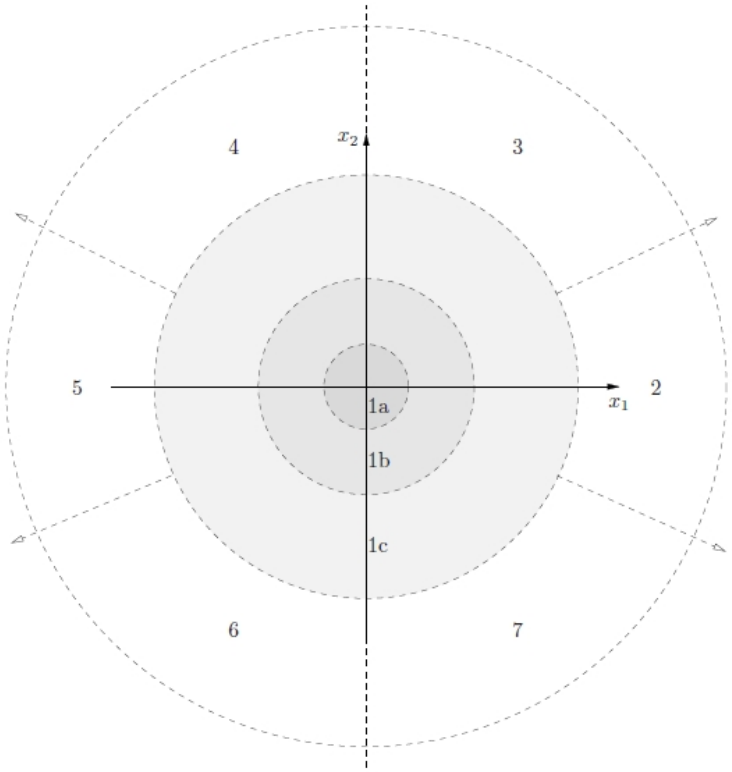

FIG. 1. *Computational domains*

For the reduced ζ we now have the equations

$$g_\zeta^{T_1}(z) = \frac{1}{2\pi} e^{-ix_1k_1} \Re \left(\int_0^{T_1} e^{ix_2t} \frac{e^{-x_1\sqrt{t^2+2tk_2i-k_1^2}}}{\sqrt{t^2+2tk_2i-k_1^2}} dt \right), \tag{4.24}$$

$$g_\zeta^{T_2}(z) = \frac{1}{2\pi} e^{-ix_1k_1} \Re \left(\int_0^{T_2} e^{-x_2t} \frac{e^{-x_1i\sqrt{t^2+2tk_2+k_1^2}}}{\sqrt{t^2+2tk_2+k_1^2}} dt \right), \quad x_2 \geq 0, \tag{4.25}$$

$$\begin{aligned} g_\zeta^{T_3}(z) = \frac{1}{2\pi} e^{-ix_1k_1} \Re \Bigg(& \int_0^{\sqrt{E}+1} e^{ix_2t} \frac{e^{-x_1\sqrt{t^2+2tk_2i-k_1^2}}}{\sqrt{t^2+2tk_2i-k_1^2}} dt \\ & -ie^{i(\sqrt{E}+1)x_2} \int_0^{T_3} e^{x_2t} \frac{e^{-x_1\sqrt{b}}}{\sqrt{b}} dt \Bigg), \quad x_2 < 0, \end{aligned} \tag{4.26}$$

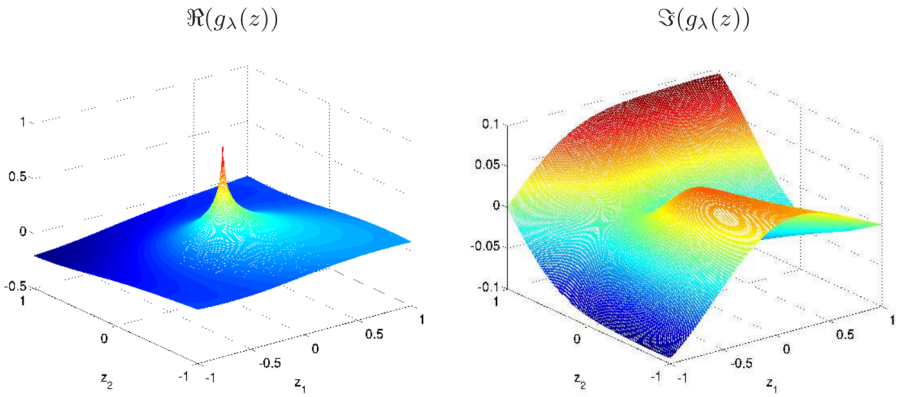

FIG. 2. *The real and imaginary parts of* $g_\lambda(z)$ *in* 400×400 *grid of points* z, $\lambda = 1 + i$, $E = 1$.

where $b = (\sqrt{E}+1+(k_2-t)\mathrm{i})^2 - E$. In general the point z lies in one of the computational domains;

- In domain 1a, we use the single-layer potential and the equation (4.23).
- In domain 1b, we scale the point z to the annulus $D_4 \setminus D_3$ using (4.2),

$$g_\zeta(z) = g_\zeta(1/5 \cdot 5x) = g_{\zeta/5}(5x)$$

  (note that the energy E changes via this scaling transformation).
- In domain 1c we do the same as above with the scaling factor 2.
- In domain 2 we use (4.24), since $|x_2|$ is small and x_1 is large. The upper limit T_1 is computed from (4.19).
- In domain 3 we use (4.25), since x_1 is small and $x_2 > 0$ is large. The upper limit T_2 is computed from (4.20).
- In domain 7 we use (4.26), since x_1 is small, $x_2 < 0$ and $|x_2|$ is large. The upper limit T_3 is computed from (4.21).
- In domains 4,5,6 we use (4.7) to switch them to domains 3,2,7 respectively.

A sample of the function $g_\lambda(z)$ is pictured in Figure 2, in 400×400 -grid of points z, $\lambda = 1 + i$, $E = 1$.

4.5.1. Domain 1a and the single-layer method explained in more detail. We take two radii $R = 1.6$ and $\epsilon = 0.1$, and divide $[0, 2\pi)$ into 256 equally distanced points forming the vector $\theta \in \mathbb{R}^{256}$. We write

$$\mathbf{y}_1 = R\mathrm{e}^{\mathrm{i}\theta} \in \mathbb{C}^{256}$$
$$\mathbf{y}_2 = (R+\epsilon)\mathrm{e}^{\mathrm{i}\theta} \in \mathbb{C}^{256},$$

where any complex element y_i refers to the point $[\Re(y_i)\ \Im(y_i)]^T$. Using the computational method for domains 2,3,4,5,6,7 we calculate $g_\zeta(\mathbf{y}_1)$, and subsequently $H_\zeta(\mathbf{y}_1) = G_\zeta(\mathbf{y}_1) - G(\mathbf{y}_1)$. In order to avoid singularities in the integral operator (4.22) we aim to calculate the single-layer potential $p(z)$ on the circle $\partial D(0, R+\epsilon)$. The integral operator can be written as a matrix,

$$S_p = d\theta(R+\epsilon)\frac{\mathrm{i}}{4}\begin{bmatrix} H_0^1(\sqrt{E}\,|y_1\mathbf{1}^T - \mathbf{y}_2{}^T|) \\ H_0^1(\sqrt{E}\,|y_2\mathbf{1}^T - \mathbf{y}_2{}^T|) \\ \vdots \\ H_0^1(\sqrt{E}\,|y_{256}\mathbf{1}^T - \mathbf{y}_2{}^T|) \end{bmatrix},$$

where $d\theta(R+\epsilon)$ comes from the numerical integration on the circle $\partial D(0, R+\epsilon)$, $d\theta = 2\pi/256$, y_i is the i:th component of $\mathbf{y}_1$ and $\mathbf{1} \in \mathbb{R}^{256}$ is a vector of ones. Now, the equation (4.22) in vector-form

is

$$H_\zeta(\mathbf{y}_1) = S_p p(\mathbf{y}_2).$$

We use GMRES to compute

$$p(\mathbf{y}_2) = S_p^{-1} H_\zeta(\mathbf{y}_1).$$

Let us be given points z_j, $1 \le j \le n$, in domain 1a. Using the complex form $z_j \in \mathbb{C}$ the matrix form of the integral operator of (4.22) is

$$S = d\theta(R+\epsilon)\frac{\mathrm{i}}{4}\begin{bmatrix} H_0^1(\sqrt{E}\,|z_1\mathbf{1}^T - \mathbf{y}_2{}^T|) \\ H_0^1(\sqrt{E}\,|z_2\mathbf{1}^T - \mathbf{y}_2{}^T|) \\ \vdots \\ H_0^1(\sqrt{E}\,|z_n\mathbf{1}^T - \mathbf{y}_2{}^T|) \end{bmatrix},$$

and so for the complex vector $z = [z_1\ z_2\ \cdots\ z_n]^T$ we have

$$H_\zeta(z) = Sp(\mathbf{y}_2)$$

and finally

$$g_\zeta(z_j) = \mathrm{e}^{-\mathrm{i}\zeta\cdot z_j}(H_\zeta(z_j) + G(z_j)), \quad 1 \le j \le n. \tag{4.27}$$

5. Numerical results. We now fix $E = 1$ and assume q_0 to be real valued. This section divides into three parts.

1. We test the algorithm for computing $g_\lambda(z)$ by computing the CGO solutions via the forward problem. For any $|\lambda| > 1$ the corresponding CGO solution $\mu(z,\lambda)$ can be computed from the Lippman-Schwinger equation (1.17) using periodic Sobolev spaces wrapped in a torus [32]. The numerical solver uses $2^M \times 2^M$ grid points of z in which the CGO solution is presented. By applying a discrete version of the $\bar\partial$ -equation (1.27) we can validate the computed CGO solutions.
2. We test the suggested numerical algorithm for computing the potential q_0 for several test potentials.
3. Using the forward problem, we compute the scattering transform for various radially symmetric potentials in search for exceptional points.

5.1. Validation of the numerical Faddeev Green's function.

5.1.1. Definition of potentials. We use exactly the same potentials as in the numerical part of [29]. Take radii $0 < r_1 < r_2 < 1$ and a polynomial $\tilde p(t) = 1 - 10t^3 + 15t^4 - 6t^5$. Set for $r_1 \le t \le r_2$

$$p(t) = \tilde p(\frac{t - r_1}{r_2 - r_1}).$$

Then, the approximate test function

$$\varphi(|z|) = \begin{cases} 1 & \text{for} \quad 0 \le |z| \le r_1 \\ p(|z|) & \text{for} \quad r_1 < |z| < r_2 \\ 0 & \text{for} \quad r_2 \le |z| \le 1, \end{cases} \tag{5.1}$$

is in C^2. The values $r_1 = 0.8$ and $r_2 = 0.9$ were used. We consider the potentials

$$\begin{array}{rcll} q_\alpha^{(1)} & = & \alpha\varphi, & \alpha \in \mathbb{R}, \\ q_\alpha^{(2)} & = & \frac{\Delta\sqrt{\sigma}}{\sqrt{\sigma}} + \alpha\varphi, & \alpha \in \mathbb{R},, \end{array} \tag{5.2}$$

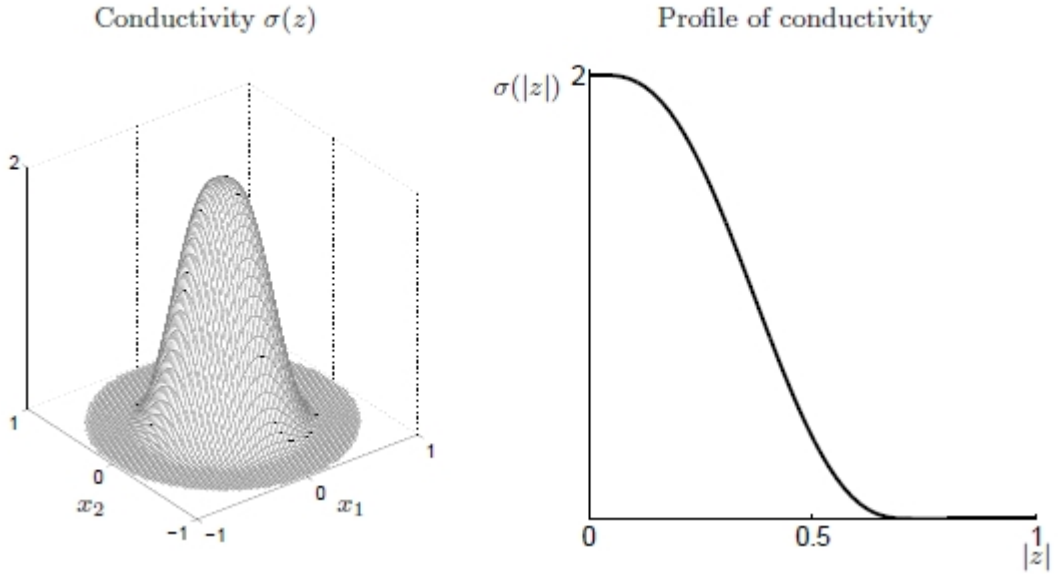

FIG. 3. *Mesh plot and profile plot of the rotationally symmetric conductivity* $\sigma(z) = \sigma(|z|)$.

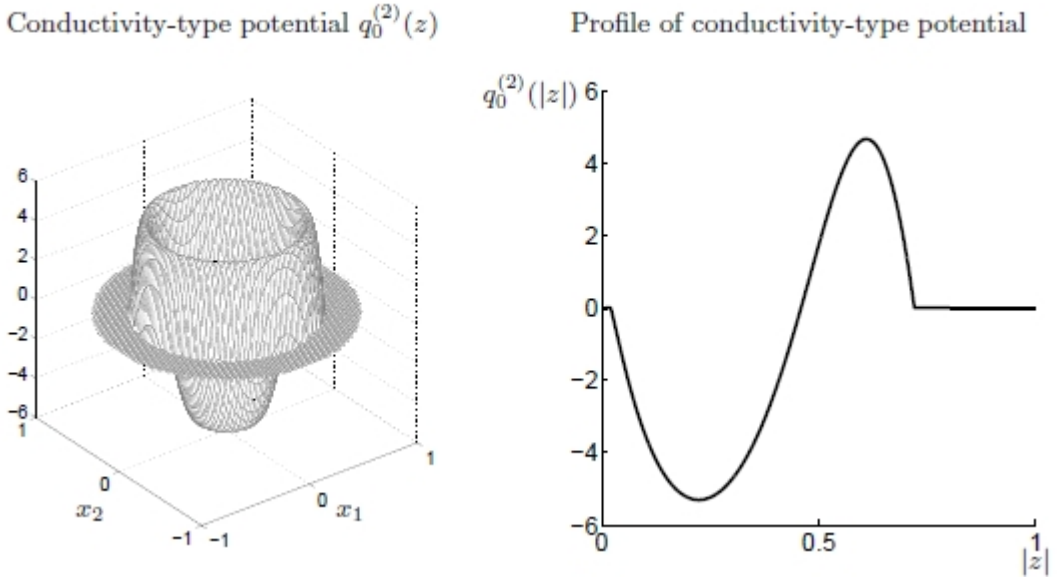

FIG. 4. *Mesh plot and profile plot of the conductivity-type potential* $q_0^{(2)}(z) = q_0^{(2)}(|z|)$.

where $\sigma \in C^2(\Omega), \sigma \geq c > 0$. The mesh plot and the profile plot of the conductivity σ are pictured in Figure 3. The conductivity-type potential $q_0^{(2)}$ and the approximate test function φ are pictured similarily in Figures 4 and 5 respectively.

Since $\|\varphi\|_{L^\infty(\mathbb{R}^2)} = 1$, using the norm-smallness condition (1.23) to $q_\alpha^{(1)}$ from (5.2), we have no exceptional points when

$$|\alpha| < \frac{1}{\hat{c}(4\pi/3 + D_\epsilon)}.$$

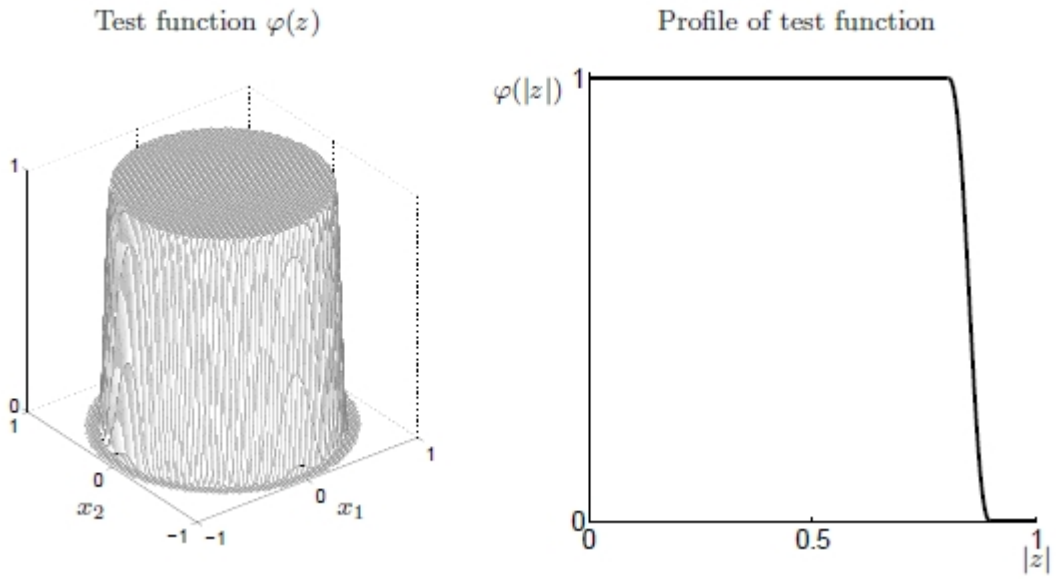

FIG. 5. *Mesh plot and profile plot of the test function* $\varphi(z) = \varphi(|z|)$.

5.1.2. Verification of the computed CGO solutions. To verify that the CGO solutions (and subsequently the Faddeev Green's function) are correct, we test the $\bar{\partial}$ -equation (1.27) using the five-point stencil method with the finite difference $d\lambda = 0.0001$. Take parameters λ from 1.01 to 4.5. Choose the potentials $q_0^{(2)}$ and $q_{35}^{(2)}$. For each $\lambda = \lambda_1 + \lambda_2 i$, compute

1. The CGO solution μ_0 in the z-grid, corresponding to the parameter λ.
2. The CGO solutions $\mu_1, \mu_2, \mu_3, \mu_4, \mu_5, \mu_6, \mu_7$ and μ_8 using $\lambda + d\lambda$, $\lambda + 2d\lambda$, $\lambda - d\lambda$, $\lambda - 2d\lambda$, $\lambda + d\lambda\mathrm{i}$, $\lambda + 2d\lambda\mathrm{i}$, $\lambda - d\lambda\mathrm{i}$ and $\lambda - 2d\lambda\mathrm{i}$ respectively.
3. The functions $e_\lambda(z)$ and $e_{-\lambda}(z)$.
4. The potential $q_0(z)$ and the scattering transform $\mathbf{t}(\lambda)$ with μ_0 using (1.26).
5. The derivatives and the $\bar{\partial}$ -operation by

$$\partial_{\lambda_1}\mu = \frac{-\mu_2 + 8\mu_1 - 8\mu_3 + \mu_4}{12d\lambda}$$
$$\partial_{\lambda_2}\mu = \frac{-\mu_6 + 8\mu_5 - 8\mu_7 + \mu_8}{12d\lambda}$$
$$\bar{\partial}\mu = \frac{1}{2}(\partial_{\lambda_1} + \mathrm{i}\partial_{\lambda_2})\mu.$$

6. The error

$$\left\| \bar{\partial}\mu - \frac{1}{4\pi\overline{\lambda}}\mathbf{t}(\lambda)e_{-\lambda}(z)\overline{\mu_0} \right\|_{L^2(D(0,1))}. \tag{5.3}$$

In Figure 6 we see the error (5.3) as a function of λ using $q_0^{(2)}$ on the left, $q_{35}^{(2)}$ on the right. The parameter M is increased from 7 to 9. As expected, the error decreases as M increases as it increases the accuracy of the LS -solver. The smallest values of λ were omitted in the pictures, for $\lambda = 1.01$ the magnitude of the error was between 3 and 13, for the second smallest λ it was between 0.003 and 0.02. For values of λ near $|\lambda| = 1$ the numerical method of $g_\lambda(z)$ has great error due to very small value of k_2, see section 4.1.1.

In the reconstruction of the potential we use values as large as $|\lambda| \approx 30$. Not pictured here, this test was done also for larger values of λ, the error seems to be of similar magnitude for any $1.01 < |\lambda| < 30$.

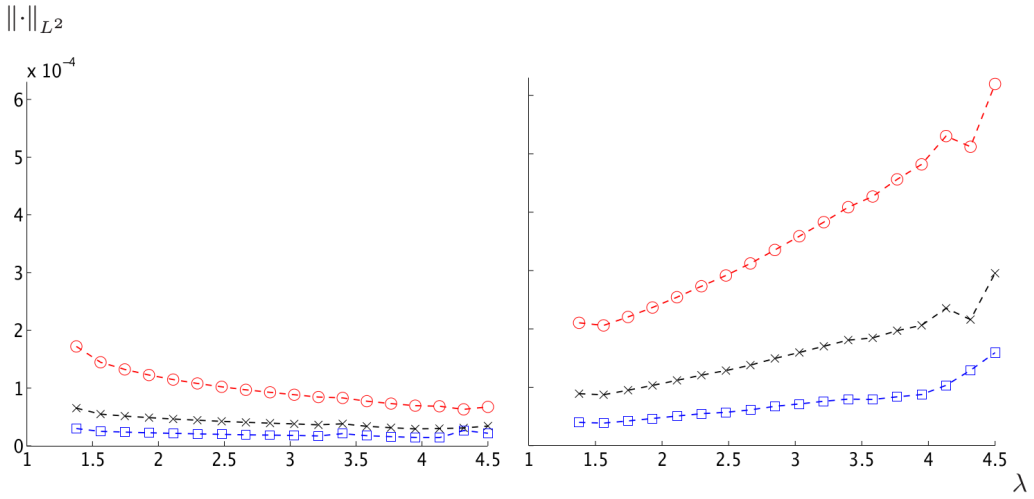

FIG. 6. *Errors in the $\bar{\partial}$ -equation for two different potentials and different accuracies of the LS -solver; horizontal axis is the spectral parameter λ, vertical axis is the norm $\left\|\bar{\partial}\mu - \frac{1}{4\pi\overline{\lambda}}\mathbf{t}(\lambda)e_{-\lambda}(z)\overline{\mu_0}\right\|_{L^2}$. On the left we used $q_0^{(2)}$ and on the right $q_{35}^{(2)}$. In red using circles is $M = 7$, in black using crosses $M = 8$ and in blue using squares is $M = 9$. Two smallest values for λ were omitted, for $\lambda = 1.01$ the magnitude of the error was between 3 and 13, for the second smallest it was between 0.003 and 0.02.*

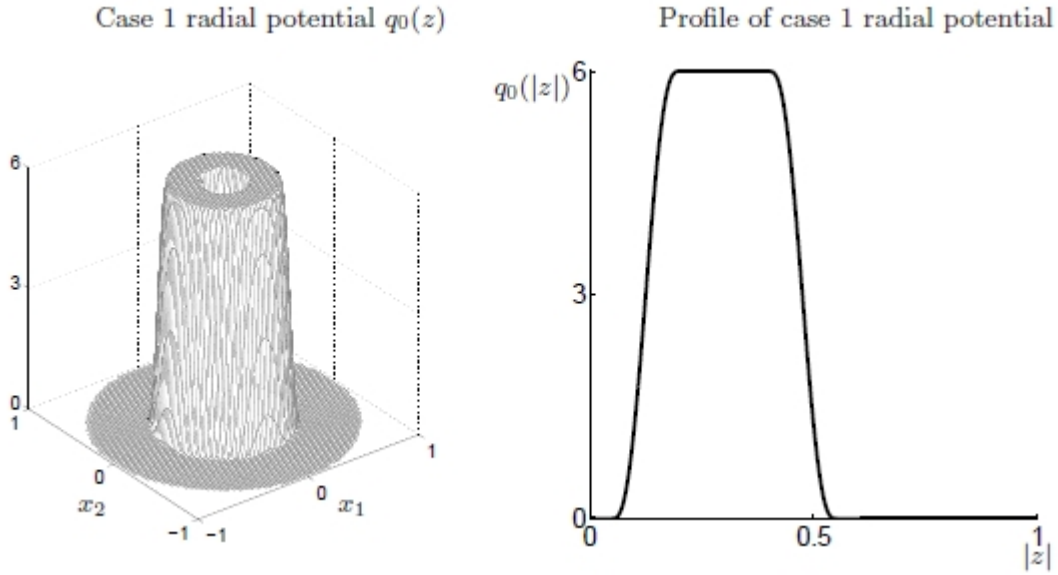

FIG. 7. *Mesh plot and profile plot of the case 1 radial potential $q_0(z) = q_0(|z|)$.*

5.2. Reconstructions of q_0. We test two radially symmetric potentials (case 1 and case 2) and one non-symmetric potential (case 3). The mesh plot and the profile plot of the former are pictured in Figures 7 and 8. The non-symmetric potential is pictured in Figure 9.

For the DN- and S_λ -matrices we use $N = 16$, see (2.3) and (3.2). We add gaussian noise to each element with (2.4) so that the relative matrix norm between the original DN-matrix and the noisy DN-matrix is 0.001%. In the mesh for the FEM we have 1048576 triangles.

For radially symmetric potentials we have $\mathbf{t}(\lambda) = \mathbf{t}(|\lambda|)$ and $\Im(\mathbf{t}(\lambda)) = 0$. In Figure 10 we have the radially symmetric scattering transform computed in three ways; black solid line indicates

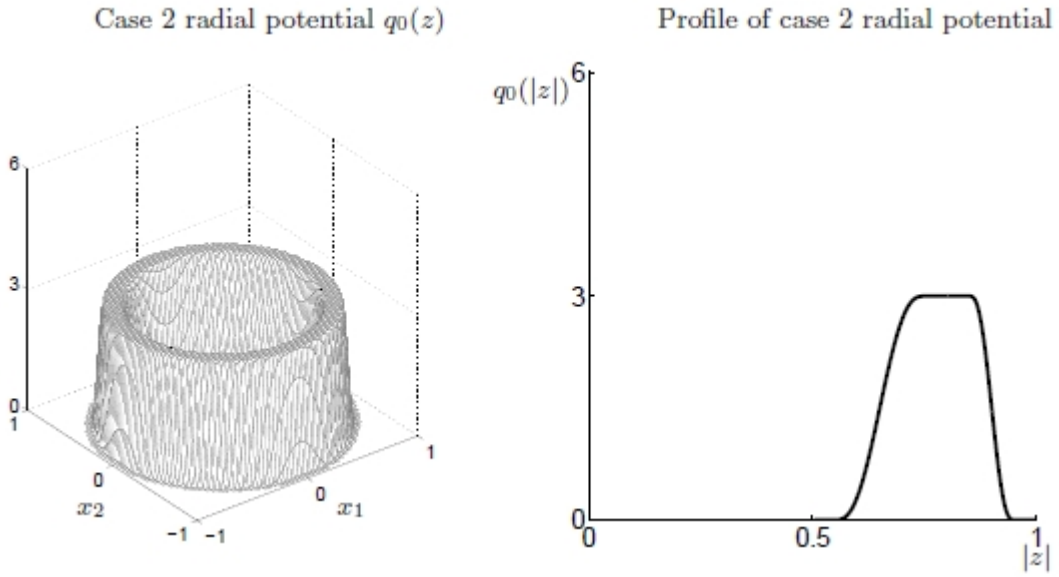

FIG. 8. *Mesh plot and profile plot of the case 2 radial potential* $q_0(z) = q_0(|z|)$.

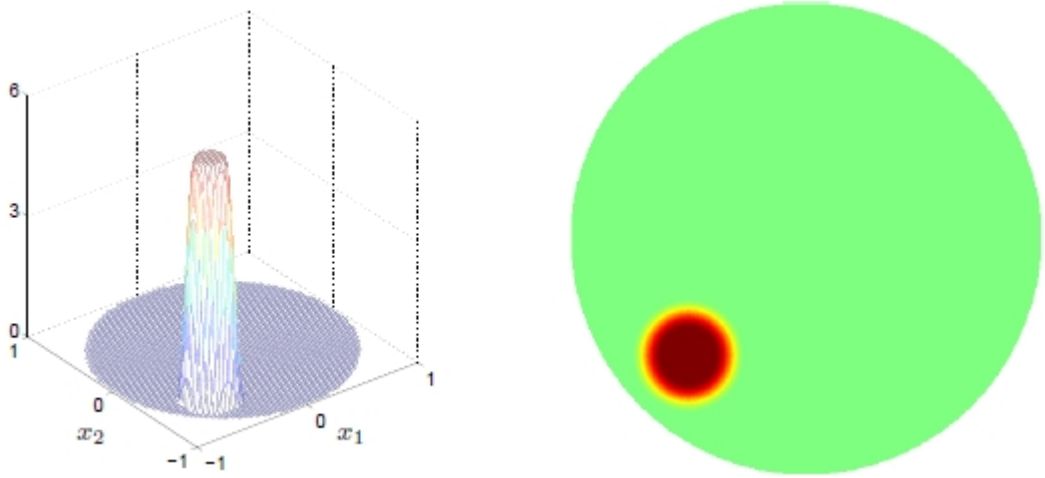

FIG. 9. *Mesh plot and 2D plot of the case 3 non-symmetric potential* $q_0(z)$.

computation directly from (1.17) using the knowledge of q_0, blue dashed line indicates computation using the DN-matrices L_q and L_{-E} and using (3.3) and (1.34), red dashed line indicates the same but with noisy DN -matrix L_q^ϵ. On the left we used case 1 potential of Figure 7 and on the right we used case 2 potential of Figure 8.

In Figure 11 we have the real and imaginary parts of the scattering transform of case 3 non-symmetric potential (see Figure 9) computed using the non-noisy DN-matrix L_q and the noisy DN-matrix L_q^ϵ. In the white areas the computation breaks down. The black line indicates the ellipse used for the truncation $\mathbf{t}_R$.

We choose $R_1 = 1.01$ to take care of problems with $|\lambda|$ close to 1. In the operator $\mathcal{M}_\epsilon$ (3.4) we choose $\epsilon = 0.011$. We solve the periodized version of the integral equation (1.31) in a $2^{M_d} \times 2^{M_d}$ -sized λ-grid. In the radial cases we use $M_d = 10$, in the non-symmetric case we use $M_d = 9$. Recall

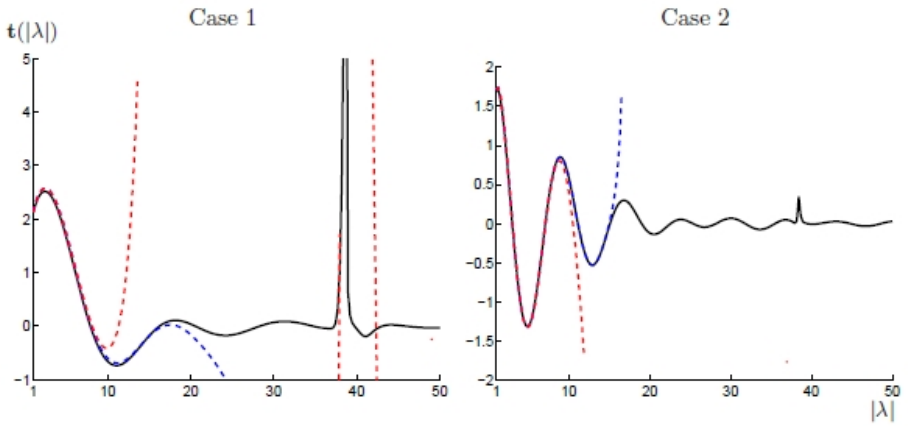

FIG. 10. *The radial scattering transform* $\mathbf{t}(|\lambda|)$ *computed in three ways; black solid line indicates computation directly from* (1.17) *using the knowledge of* q_0*, blue dashed line indicates computation using the DN-matrices* L_q*,* L_{-E} *and using equations* (3.3) *and* (1.34)*, red dashed line indicates the same but with noisy DN-matrix* L_q^ϵ*.*

the formula for an ellipse (3.1). Based on Figures 10 and 11 we choose

- for cases 1 and 2 using the scattering transform computed directly from the potentials, $a = b = 30$, $\phi = 0$,
- for cases 1 and 2 using the DN-maps without noise $a = b = 15$, $\phi = 0$,
- for cases 1 and 2 using the DN-maps with noise $a = b = 8$, $\phi = 0$,
- for case 3 using the DN-map without noise we choose $a = 16$, $b = 12$,$\phi = \pi/4$,
- for case 3 using the DN-map with noise we choose $a = 11$, $b = 11$,$\phi = 0$.

In Figure 12 we plot the reconstructions of cases 1 and 2 using the three different scattering transforms. Black solid line indicates the original potential, black dashed line indicates the reconstruction using the knowledge of the potential via the scattering transform (1.26), blue dashed line indicates reconstruction using (3.5) without noise, and red dashed line indicates reconstruction using (3.5) with added noise.

In Figure 13 we picture the original case 3 potential on the left, the reconstruction using (3.5) without noise in the middle and the reconstruction using (3.5) with added noise on the right. Relative errors $\|q_0 - q_{\rm rec}\|_{L^2(\Omega)} / \|q_0\|_{L^2(\Omega)}$, where $q_{\rm rec}$ is the reconstruction, are given.

5.3. Numerical investigation of exceptional points. Recall the potentials $q_\alpha^{(1)}$ and $q_\alpha^{(2)}$ from (5.2), see Figures 3, 4 and 5. We use 250 discrete points of λ and 701 discrete points of α,

$$\lambda = 1.01, .., 4.5, \quad \alpha = -35, ..., 35.$$

We use $M = 8$ for the LS -solver leading to $2^M \times 2^M$ sized z-grid. In Figure 14 we plot the radially symmetric and real-valued scattering transform $\mathbf{t}(\lambda)$ for the potential $q_\alpha^{(1)} = \alpha\varphi$; the x-axis is the parameter α and the y-axis is the spectral parameter λ. In Figure 15 we have the same for $q_\alpha^{(2)} = q_\gamma + \alpha\varphi$. Black color represents very small negative values, and white very large positive values of $\mathbf{t}(\lambda)$. The lines where it abruptly changes between these colors are exceptional circles that move as the parameter α changes.

In Figure 16 we plot the profile of the scattering transform $\mathbf{t}(\lambda)$ as a function of λ, using the potential $q_\alpha^{(1)} = \alpha\psi$, with the values $\alpha = -5, -15, -30$. The exceptional circles can be seen as singularities in the profiles.

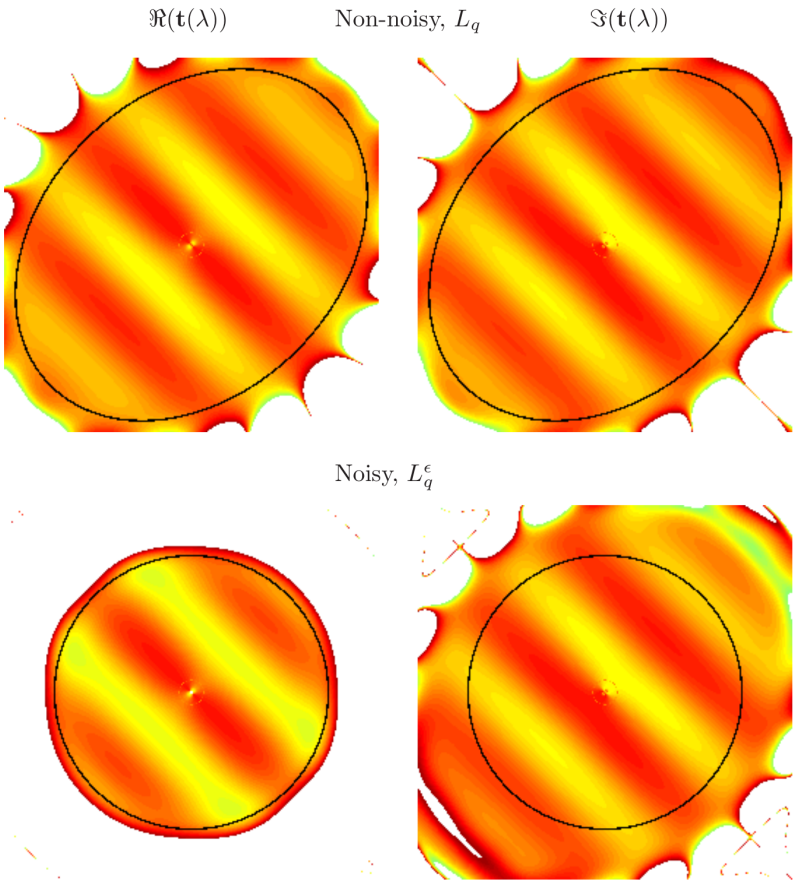

FIG. 11. *The scattering transform* $\mathbf{t}(\lambda)$ *of case 3, the non-symmetric potential of Figure 9. Real part on the left, imaginary part on the right, in a* λ *-grid* $[-15,15]\times[-15,15]i$*. On the top row: the non-noisy DN-matrix* L_q *was used. On the bottom row: the noisy DN-matrix* L_q^ϵ *was used. In the white areas the computation breaks down. The black line indicates the ellipse used for the truncation* $\mathbf{t}_R(\lambda)$*.*

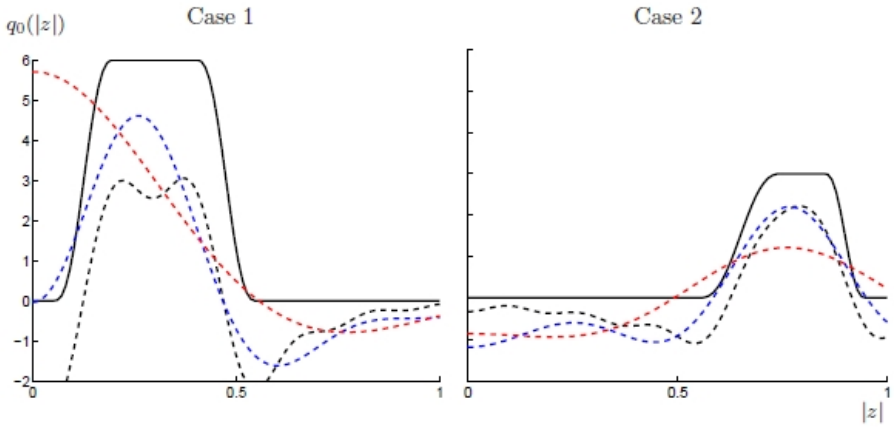

FIG. 12. *Reconstruction of the potentials* $q_0(|z|)$*. Black solid line: the original potential. Black dashed line: reconstruction using the knowledge of the potential via the scattering transform* (1.26)*. Blue dashed line: reconstruction using the new computational method without noise. Red dashed line: reconstruction using the new computational method with added noise.*

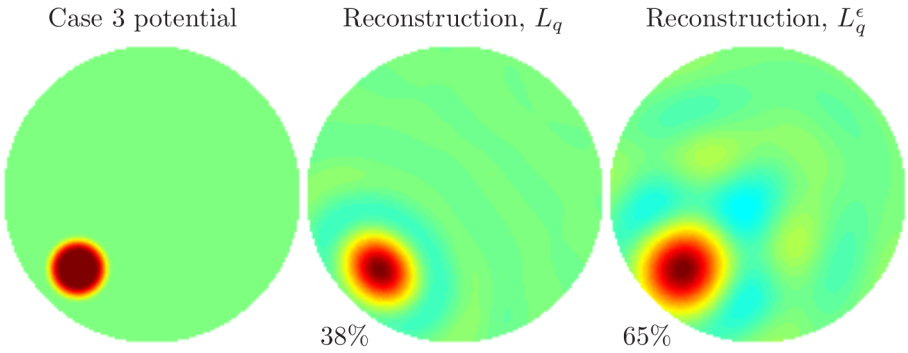

FIG. 13. *On the left: the original case 3 potential, see Figure 9. In the middle: reconstruction using the non-noisy DN-matrix L_q. On the right: reconstruction using the noisy DN-matrix L_q^ϵ. Relative errors $\|q_0 - q_{rec}\|_{L^2(\Omega)} / \|q_0\|_{L^2(\Omega)}$ are given.*

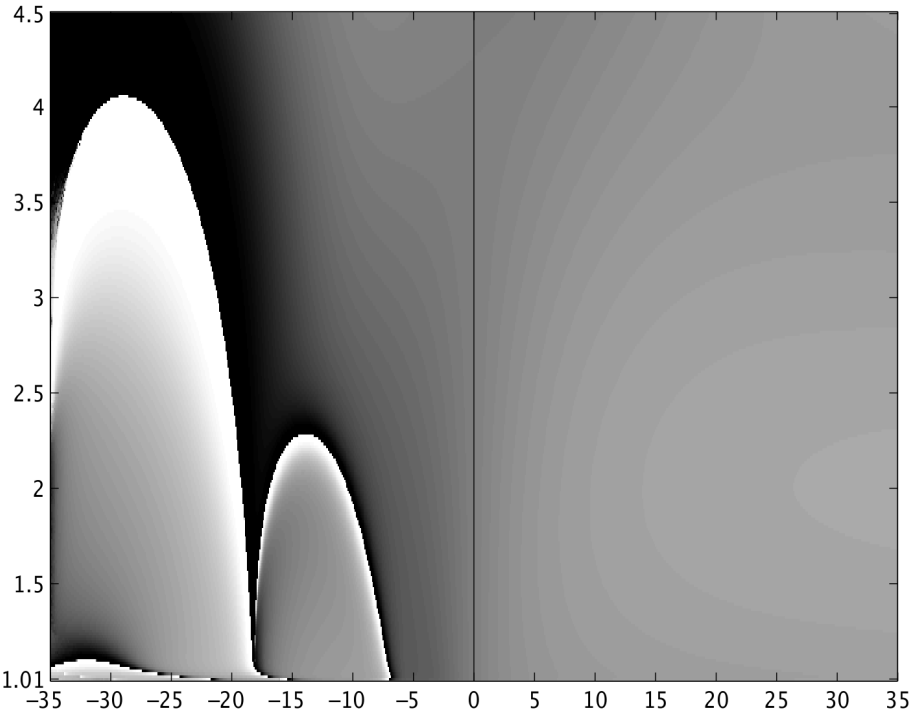

FIG. 14. *Scattering transform for the potential $q_\alpha^{(1)} = \alpha\varphi$; x-axis is $\alpha = -35..35$, y-axis is $\lambda = 1.01..4.5$*

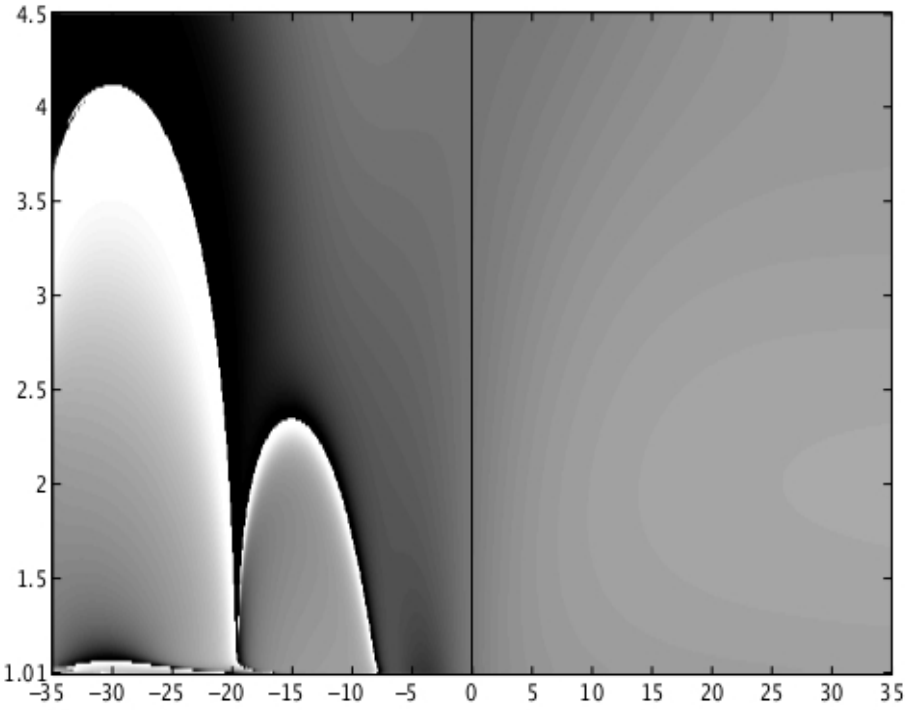

FIG. 15. *Scattering transform for the potential* $q_\alpha^{(2)} = q_\gamma + \alpha\varphi$*; x-axis is* $\alpha = -35..35$*, y-axis is* $\lambda = 1.01..4.5$

6. Conclusions. We developed a new numerical method for reconstructing the potential from boundary measurements in the Gel'fand-Dirichlet problem. The method seems to work as evidenced by the reconstructions, even if the theory is still missing details. The use of an ellipse as a truncation shape is obvious from the scattering images, but this unsymmetry in the scattering transform is a new phenomenon compared to the zero-energy case. During the numerical testing it was also noted that the operator $\mathcal{M}_\epsilon$ had only minor effect in the reconstructions in the test potentials used.

The numerical method for g_λ is not accurate near $|\lambda| = 1$ which resulted in high errors in the verification test of Figure 6 using the $\bar{\partial}$ -equation.

The numerical evidence show no exceptional points for small α nor for large λ, which was expected from the result of section 1.3.1. Also according to our tests there are no exceptional points for positive α. For negative α, there are either one or two exceptional circles in the range of parameters investigated. The two types of potentials $q_\alpha^{(1)}$ and $q_\alpha^{(2)}$ have little difference in their exceptional points, mainly in the second exceptional circle forming at $\alpha = -20$ as α is decreased from zero.

Acknowledgements. JPT was supported in part by Suomen Kulttuurirahasto and European Research Council (ERC) Advanced Grant.

REFERENCES

[1] MICHEL ASSENHEIMER, ORAH LAVER-MOSKOVITZ, DOV MALONEK, DAVID MANOR, UDI NAHALIEL, RON NITZAN, AND ABRAHAM SAAD, *The t-scan tm technology: electrical impedance as a diagnostic tool for breast cancer detection*, Physiological Measurement, 22 (2001), pp. 1–8.

[2] KARI ASTALA, JENNIFER L. MUELLER, LASSI PÄIVÄRINTA, ALLAN PERÄMÄKI, AND S. SILTANEN., *Direct electrical impedance tomography for nonsmooth conductivities*, Inverse Problem, 5 (2011), pp. 531–549.

[3] KARI ASTALA, JENNIFER L. MUELLER, LASSI PÄIVRINTA, AND SAMULI SILTANEN, *Numerical computation of complex geometrical optics solutions to the conductivity equation*, Applied and Computational Harmonic

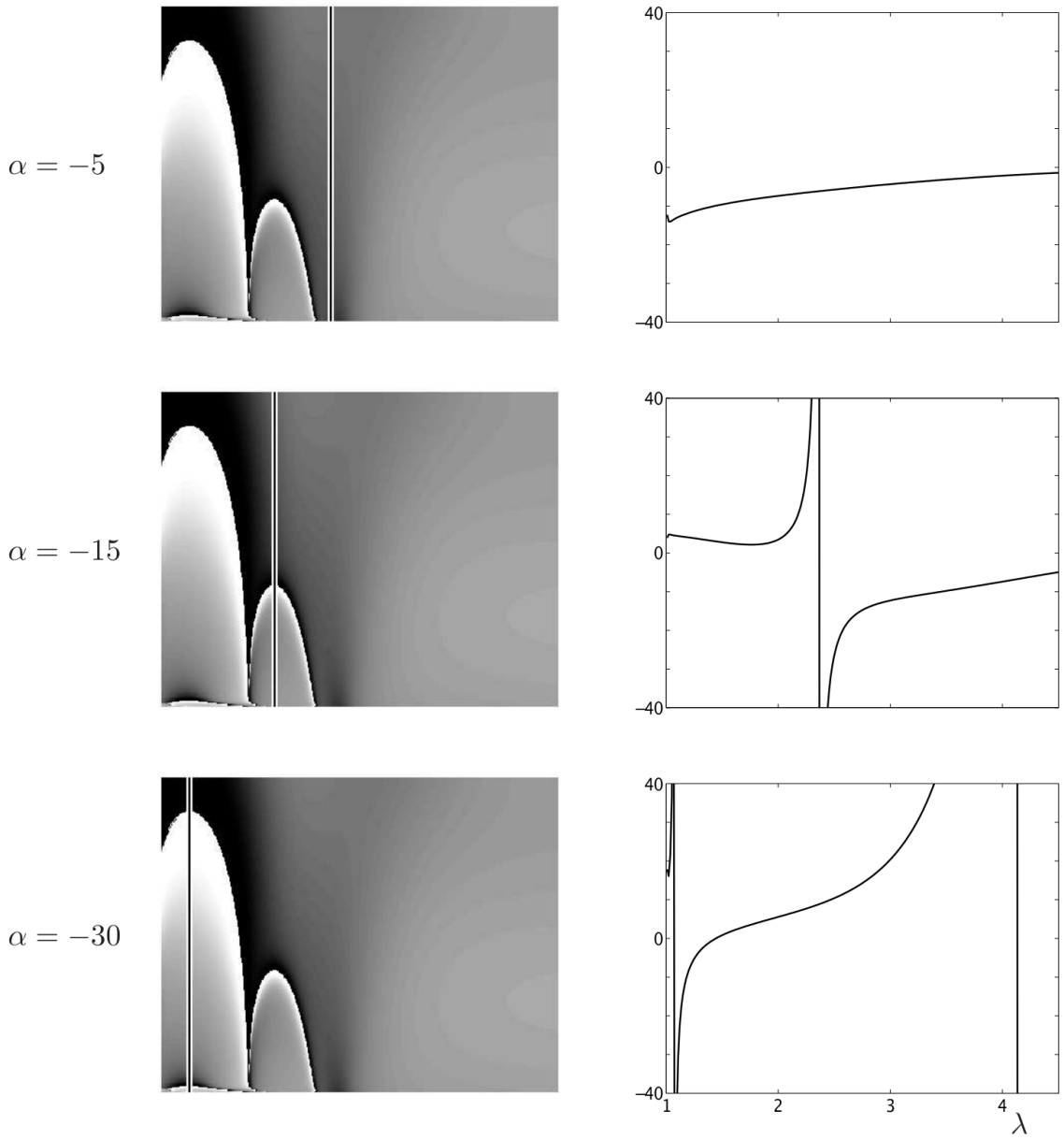

FIG. 16. *On the right: the profile of* $\mathbf{t}(\lambda)$ *as a function of* λ *using the potential* $q_\alpha^{(1)} = \alpha\varphi$ *with three different values of* α*. On the left: the plane* $\mathbf{t}(\lambda)$ *for all parameters* α *with an indication of the location of the profile on the right.*

Analysis, 29 (2010), pp. 391–403.

[4] KARI ASTALA AND LASSI PÄIVÄRINTA, *A boundary integral equation for calderón's inverse conductivity problem*, Annals of Mathematics, 163 (2006), pp. 265–299.

[5] ———, *A boundary integral equation for calderón's inverse conductivity problem*, Conference on Harmonic Analysis, Collectanea Mathematica, (2006).

[6] COIFMAN R. BEALS, R., *Scattering, transformations spectrales et équations dévolution non linaire ii*, Sminaire quations aux drives partielles (dit "Goulaouic-Schwartz"), (1981).

[7] RUSSELL M. BROWN, GUNTHER UHLMANN, AND SOBOLEV SPACE H, *Uniqueness in the inverse conductivity problem for nonsmooth conductivities in two dimensions*, Communications in Partial Differential Equations, 22 (1997), pp. 1009–1027.

[8] ALBERTO P. CALDERÓRN, *On an inverse boundary value problem*, Seminar on Numerical Analysis and its

Applications to Continuum Physics (Rio de Janeiro), (1980), pp. 65–73.
[9] Margaret Cheney, David Isaacson, and Jonathan C. Newell, *Electrical impedance tomography*, SIAM Review, 41 (1999), pp. 85–101.
[10] L. D. Faddeev, *Increasing solutions of the schrodinger equation*, Soviet Physics Doklady, 10 (1966), pp. 1033–1035.
[11] I. M. Gelfand, *Some problems of functional analysis and algebra*, International Mathematical Congress in Amsterdam (in Russian), (1961), pp. 49–74.
[12] P.G. Grinevich and S.V. Manakov, *Inverse scattering problem for the two-dimensional schrdinger operator, the $\bar{\partial}$-method and nonlinear equations*, Functional Analysis and Its Applications, 20 (1986), pp. 94–103.
[13] P G Grinevich, *Scattering transformation at fixed non-zero energy for the two-dimensional schrdinger operator with potential decaying at infinity*, Russian Mathematical Surveys, 55 (2000), pp. 1015–1083.
[14] S. J. Hamilton, C. N. L. Herrera, J. L. Mueller, and A. Von Herrmann, *A direct d-bar reconstruction algorithm for recovering a complex conductivity in 2d*, Inverse Problems, 28 (2012), p. 095005.
[15] D. Isaacson, J.L. Mueller, J.C. Newell, and S. Siltanen, *Reconstructions of chest phantoms by the d-bar method for electrical impedance tomography*, Medical Imaging, IEEE Transactions on, 23 (2004), pp. 821–828.
[16] D Isaacson, J L Mueller, J C Newell, and S Siltanen, *Imaging cardiac activity by the d-bar method for electrical impedance tomography*, Physiological Measurement, 27 (2006), pp. S43–S50.
[17] Kim Knudsen, *A new direct method for reconstructing isotropic conductivities in the plane*, Physiological Measurement, 24 (2003), pp. 391–403.
[18] Kim Knudsen, Matti Lassas, Jennifer Mueller, and Samuli Siltanen, *Regularized d-bar method for the inverse conductivity problem*, Inverse Problems and Imaging, 3 (2009), pp. 599–624.
[19] K. Knudsen, J. Mueller, and S. Siltanen, *Numerical solution method for the dbar-equation in the plane*, J. Comput. Phys., 198 (2004), pp. 500–517.
[20] Kim Knudsen and Alexandru Tamasan, *Reconstruction of less regular conductivities in the plane*, Communications in Partial Differential Equations, 29 (2004), pp. 361–381.
[21] Jennifer L. Mueller and Samuli Siltanen, *Direct reconstructions of conductivities from boundary measurements*, SIAM J. Sci. Comput., 24 (2003), pp. 1232–1266.
[22] ———, *Linear and Nonlinear Inverse Problems with Practical Applications*, Society for Industrial and Applied Mathematics, Philadelphia, PA, USA, 2012.
[23] M Music, P Perry, and S Siltanen, *Exceptional circles of radial potentials*, Inverse Problems, 29 (2013), p. 045004.
[24] Adrian Nachman, John Sylvester, and Gunther Uhlmann, *An n-dimensional borg-levinson theorem*, Communications in Mathematical Physics, 115 (1988), pp. 595–605.
[25] Adrian I. Nachman, *Global Uniqueness for a Two-Dimensional Inverse Boundary Value Problem*, The Annals of Mathematics, 143 (1996), pp. 71–96.
[26] R.G. Novikov, *Reconstruction of a two-dimensional schrdinger operator from the scattering amplitude for fixed energy*, Functional Analysis and Its Applications, 20 (1986), pp. 246–248.
[27] ———, *Multidimensional inverse spectral problem for the equation + (v(x) eu(x)) = 0*, Functional Analysis and Its Applications, 22 (1988), pp. 263–272.
[28] R.G. Novikov, *The inverse scattering problem on a fixed energy level for the two-dimensional schrödinger operator*, Journal of Functional Analysis, 103 (1992), pp. 409 – 463.
[29] P. A. Perry, *Miura maps and inverse scattering for the novikov-veselov equation*, ArXiv e-prints, (2012).
[30] Samuli Siltanen, *Electrical impedance tomography and faddeev greens functions*, Annales Academiae Scientiarum Fennicae Mathematica Dissertationes, 121 (1999), p. 56.
[31] Samuli Siltanen, Jennifer Mueller, and David Isaacson, *An implementation of the reconstruction algorithm of a nachman for the 2d inverse conductivity problem*, Inverse Problems, 16 (2000), pp. 681–699.
[32] Gennadi Vainikko, *Fast solvers of the lippmann-schwinger equation*, in Direct and Inverse Problems of Mathematical Physics, RobertP. Gilbert, Joji Kajiwara, and YongzhiS. Xu, eds., vol. 5 of International Society for Analysis, Applications and Computation, Springer US, 2000, pp. 423–440.